

1 Harmonization of resting-state functional MRI data across multiple imaging sites 2 via the separation of site differences into sampling bias and measurement bias

3

4 Ayumu Yamashita^{1,*}, Noriaki Yahata^{1,2,3}, Takashi Itahashi⁴, Giuseppe Lisi¹, Takashi Yamada^{1,4}, Naho
5 Ichikawa⁵, Masahiro Takamura⁵, Yujiro Yoshihara⁶, Akira Kunimatsu^{7,8}, Naohiro Okada^{2,9}, Hirotaka
6 Yamagata¹⁰, Koji Matsuo^{10,11}, Ryuichiro Hashimoto^{1,4,12}, Go Okada⁵, Yuki Sakai^{1,13}, Jun Morimoto¹,
7 Jin Narumoto^{1,13}, Yasuhiro Shimada¹⁴, Kiyoto Kasai^{1,2,9}, Nobumasa Kato^{1,4}, Hidehiko Takahashi⁶,
8 Yasumasa Okamoto⁵, Saori C Tanaka¹, Mitsuo Kawato¹, Okito Yamashita^{1,15,*}, and Hiroshi
9 Imamizu^{1,16,*}

10

11 ¹ Brain Information Communication Research Laboratory Group, Advanced Telecommunications
12 Research Institutes International, Kyoto, Japan

13 ² Department of Neuropsychiatry, Graduate School of Medicine, The University of Tokyo, Tokyo, Japan

14 ³ Department of Molecular Imaging and Theranostics, National Institute of Radiological Sciences,
15 National Institutes for Quantum and Radiological Science and Technology, Chiba, Japan

16 ⁴ Medical Institute of Developmental Disabilities Research, Showa University, Tokyo, Japan

17 ⁵ Department of Psychiatry and Neurosciences, Hiroshima University, Hiroshima, Japan

18 ⁶ Department of Psychiatry, Kyoto University Graduate School of Medicine, Kyoto, Japan

19 ⁷ Department of Radiology, IMSUT Hospital, Institute of Medical Science, The University of Tokyo,
20 Tokyo, Japan

21 ⁸ Department of Radiology, Graduate School of Medicine, The University of Tokyo, Tokyo, Japan

22 ⁹ The International Research Center for Neurointelligence (WPI-IRCN) at the University of Tokyo
23 Institutes for Advanced Study (UTIAS), Tokyo, Japan

24 ¹⁰ Division of Neuropsychiatry, Department of Neuroscience, Yamaguchi University Graduate School of
25 Medicine, Yamaguchi, Japan

26 ¹¹ Department of Psychiatry, Faculty of Medicine, Saitama Medical University, Saitama, Japan

27 ¹² Department of Language Sciences, Tokyo Metropolitan University, Tokyo, Japan

28 ¹³ Department of Psychiatry, Graduate School of Medical Science, Kyoto Prefectural University of
29 Medicine, Kyoto, Japan

30 ¹⁴ Brain Activity Imaging Center, ATR-Promotions Inc., Kyoto, Japan

31 ¹⁵ Center for Advanced Intelligence Project, RIKEN, Tokyo, Japan

32 ¹⁶ Department of Psychology, Graduate School of Humanities and Sociology, The University of Tokyo,
33 Tokyo, Japan

34

35 * **Correspondence:** imamizu@gmail.com (H.I.), oyamashi@atr.jp (O.Y.), or ayumu722@gmail.com
36 (A.Y.)

37

38 **Abstract**

39 When collecting large neuroimaging data associated with psychiatric disorders, images
40 must be acquired from multiple sites because of the limited capacity of a single site.

41 However, site differences represent the greatest barrier when acquiring multi-site
42 neuroimaging data. We utilized a traveling-subject dataset in conjunction with a multi-

43 site, multi-disorder dataset to demonstrate that site differences are composed of biological
44 sampling bias and engineering measurement bias. Effects on resting-state functional MRI

45 connectivity because of both bias types were greater than or equal to those because of

46 psychiatric disorders. Furthermore, our findings indicated that each site can sample only
47 from among a subpopulation of participants. This result suggests that it is essential to
48 collect large neuroimaging data from as many sites as possible to appropriately estimate
49 the distribution of the grand population. Finally, we developed a novel harmonization
50 method that removed only the measurement bias by using traveling-subject dataset and
51 achieved the reduction of the measurement bias by 29% and the improvement of the
52 signal to noise ratios by 40%.

53

54

55

56

57

58

59

60

61

62

63

64

65

66

67

68

69

70

71

72

73

74

75

76

77

78 **Introduction**

79 Acquiring and sharing large neuroimaging data have recently become critical for bridging
80 the gap between basic neuroscience research and clinical applications such as the
81 diagnosis and treatment of psychiatric disorders (Human Connectome Project (HCP) [1],
82 [<http://www.humanconnectomeproject.org/>]; Human Brain Project
83 [<https://www.humanbrainproject.eu/en/>]; UK Biobank [<http://www.ukbiobank.ac.uk/>];
84 and Strategic Research Program for Brain Sciences (SRPBS) [2]
85 [https://www.amed.go.jp/program/list/01/04/001_nopro.html]) [3-5]. When collecting
86 large data associated with psychiatric disorders, it is necessary to acquire images from
87 multiple sites because it is nearly impossible for a single site to collect large neuroimaging
88 data (Connectomes Related to Human Disease (CRHD),
89 [<https://www.humanconnectome.org/disease-studies>]; Autism Brain Imaging Data
90 Exchange (ABIDE); and SRPBS) [2, 6-8]. In 2013, the Japan Agency for Medical
91 Research and Development (AMED) organized the Decoded Neurofeedback (DecNef)
92 Project. The project determined the unified imaging protocol on 28th February 2014
93 (<http://www.cns.atr.jp/rs-fmri-protocol-2>) and have collected multisite resting-state
94 functional magnetic resonance imaging (rs-fMRI) data using twelve scanners across eight
95 research institutes for recent five years. The collected dataset encompasses 2,239 samples
96 and five disorders and is publicly shared through the SRPBS multisite multi-disorder
97 database (<https://bicr-resource.atr.jp/decnefpro/>). This project has enabled the
98 identification of resting-state functional connectivity (rs-fcMRI)-based biomarkers of
99 several psychiatric disorders that can be generalized to completely independent cohorts
100 [2, 8-10]. However, multisite dataset with multiple disorders raises difficult problems
101 never included in a single-site based dataset of healthy population (e.g., HCP and UK
102 Biobank). That is, our experience in the SRPBS database demonstrated difficulty in fully
103 control of scanner type, imaging protocol, patient demographics [10-13] even if the
104 unified protocol is determined. Moreover, there often exists unpredictable difference in
105 participant population among sites. Therefore, researchers must work with heterogeneous
106 neuroimaging data. In particular, site differences represent the greatest barrier when
107 extracting disease factors by applying machine-learning techniques to such
108 heterogeneous data [14] because disease factors tend to be confounded with site factors
109 [2, 8, 10-13, 15]. This confounding occurs because a single site (or hospital) is apt to

110 sample only a few types of psychiatric disorders (e.g., primarily schizophrenia from site
111 A and primarily autism spectrum disorder from site B). To properly manage such
112 heterogeneous data, it is necessary to harmonize the data among the sites [16-19].
113 Moreover, a deeper understanding of these site differences is essential for efficient
114 harmonization of the data.

115 Site differences essentially consist of two types of biases: engineering bias (i.e.,
116 measurement bias) and biological bias (i.e., sampling bias). Measurement bias includes
117 differences in the properties of MRI scanners such as imaging parameters, field strength,
118 MRI manufacturers, and scanner models, whereas sampling bias refers to differences in
119 participant groups among sites. Previous studies have investigated the effect of
120 measurement bias on resting-state functional connectivity by using a traveling-subject
121 design [20] wherein multiple participants travel to multiple sites for the assessment of
122 measurement bias [7]. By contrast, researchers to date have only speculated with regard
123 to sampling bias. For example, differences in the clinical characteristics of patients
124 examined at different sites are presumed to underlie the stagnant accuracy of certain
125 biomarkers, even after combining the data from multiple sites [12]. Furthermore, to our
126 knowledge, no study has mathematically defined sampling bias or conducted quantitative
127 analyses of its effect size, which is likely because the decomposition of site differences
128 into measurement bias and sampling bias is a complex process. To achieve this aim, we
129 combined a separate traveling-subject rs-fMRI dataset with the SRPBS multi-disorder
130 dataset. Simultaneous analysis of the datasets enabled us to divide site differences into
131 measurement bias and sampling bias and to quantitatively compare their effect sizes on
132 resting-state functional connectivity with those of psychiatric disorders.

133 Furthermore, our detailed analysis of measurement and sampling biases enabled
134 us to investigate the origin of each bias in multisite datasets for the first time. For
135 measurement bias, we quantitatively compared the magnitude of the effects among the
136 different imaging parameters, fMRI manufacturers, and number of coils in each fMRI
137 scanner. We further examined two alternative hypotheses regarding the mechanisms
138 underlying sampling bias: one hypothesis assumes that each site samples subjects from a
139 common population. In this situation, sampling bias occurs because of the random
140 sampling of subjects, which results in incidental differences in the patients' characteristics
141 among the sites. The second hypothesis assumes that each site samples subjects from

142 different subpopulations. In this situation, sampling bias occurs because of sampling from
143 subpopulations with different characteristics. For example, assume multiple sites plan to
144 collect data from the same population of patients with major depressive disorder.
145 Subtypes of major depressive disorder exist within the population such as atypical
146 depression and melancholic depression [21, 22]; therefore, one subpopulation may
147 contain a large proportion of patients with atypical depression, whereas another
148 subpopulation may contain a large proportion of patients with melancholic depression.
149 Therefore, in some instances, atypical depression may be more frequent among patients
150 at site A, whereas melancholic depression may be more frequent among patients at site
151 B. The basic protocol for collecting large-scale datasets differ between these two
152 hypotheses; thus, it is necessary to determine the hypothesis that most appropriately
153 reflects the characteristics of the SRPBS dataset. In the former situation, one would
154 simply need to collect data from a large number of subjects, even with a small number of
155 sites. In the latter situation, a larger number of sites would be required to obtain truly
156 representative data.

157 To overcome these limitations associated with site differences, we developed a
158 novel harmonization method that enabled us to subtract only the measurement bias by
159 using a traveling-subject dataset. We investigated that how much our proposed method
160 could reduce the measurement bias and could improve the signal to noise ratio. We
161 compared its performance to those of other commonly used harmonization methods. All
162 data utilized in this study can be downloaded publicly from the DecNef Project Brain
163 Data Repository at <https://bicy-resource.atr.jp/decnefpro/>.

164

165 **Results**

166 **Datasets**

167 We used two rs-fMRI datasets: the (1) SRPBS multi-disorder dataset, (2) a traveling-
168 subject dataset.

169

170 *SRPBS multi-disorder dataset*

171 This dataset included patients with five different disorders and healthy controls (HCs)
172 who were examined at nine sites belonging to eight research institutions. A total of 805
173 participants were included: 482 HCs from nine sites, 161 patients with major depressive

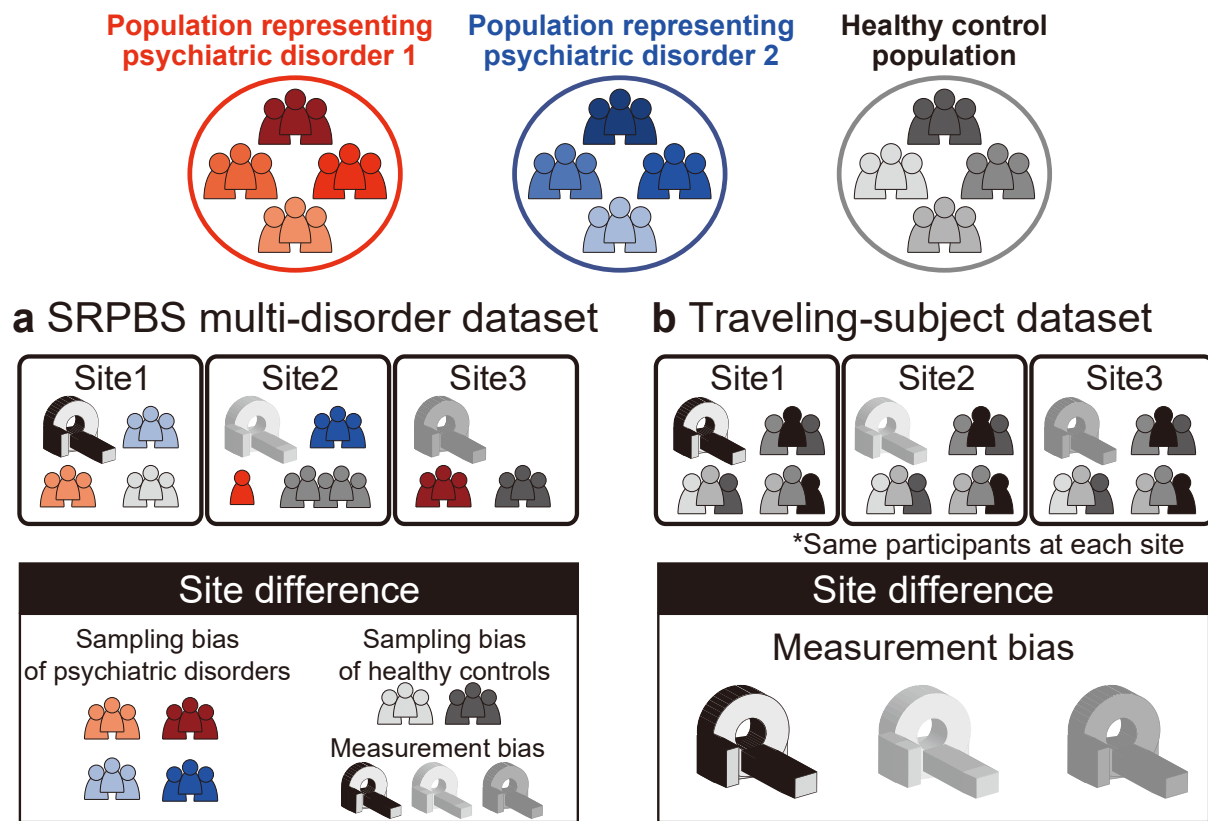
174 disorder (MDD) from five sites, 49 patients with autism spectrum disorder (ASD) from
175 one site, 65 patients with obsessive-compulsive disorder (OCD) from one site, and 48
176 patients with schizophrenia (SCZ) from three sites (Supplementary Table 1). The rs-fMRI
177 data were acquired using a unified imaging protocol at all but three sites (Supplementary
178 Table 2; <http://www.cns.atr.jp/rs-fmri-protocol-2/>). Site differences in this dataset
179 included both measurement and sampling biases (Fig. 1a). For bias estimation, we only
180 used data obtained using the unified protocol. (Patients with OCD were not scanned using
181 this unified protocol; therefore, the disorder factor could not be estimated for OCD.)

182

183 *Traveling-subject dataset*

184 We acquired a traveling-subject dataset to estimate measurement bias across sites in the
185 SRPBS dataset. Nine healthy participants (all men; age range: 24–32 years; mean age:
186 27 ± 2.6 years) were scanned at each of 12 sites, which included the nine sites in the SRPBS
187 dataset, and produced a total of 411 scan sessions (see “Participants” in the Methods
188 section). Although we had attempted to acquire this dataset using the same imaging
189 protocol as that in the SRPBS multi-disorder dataset, there were some differences in the
190 imaging protocol across sites because of limitations in parameter settings or the scanning
191 conventions of each site (Supplementary Table 3). There were two phase-encoding
192 directions (P→A and A→P), three MRI manufacturers (Siemens, GE, and Philips), four
193 numbers of coil channels (8, 12, 24, and 32), and seven scanner types (TimTrio, Verio,
194 Skyra, Spectra, MR750W, SignaHDxt, and Achieva). Site differences in this dataset
195 included measurement bias only as the same nine participants were scanned across the 12
196 sites (Fig. 1b).

197



198

199 **Figure 1: Schematic examples illustrating the two main datasets.**

200 (a) The SRPBS multi-disorder dataset includes patients with psychiatric disorders and healthy
201 controls. The number of patients and scanner types differed among sites. Thus, site differences
202 consist of sampling bias and measurement bias. (b) The traveling-subject dataset includes only
203 healthy controls, and the participants were the same across all sites. Thus, site differences
204 consist of measurement bias only. SRPBS: Strategic Research Program for Brain Sciences.

205

206

207

208

209

210

211

212

213

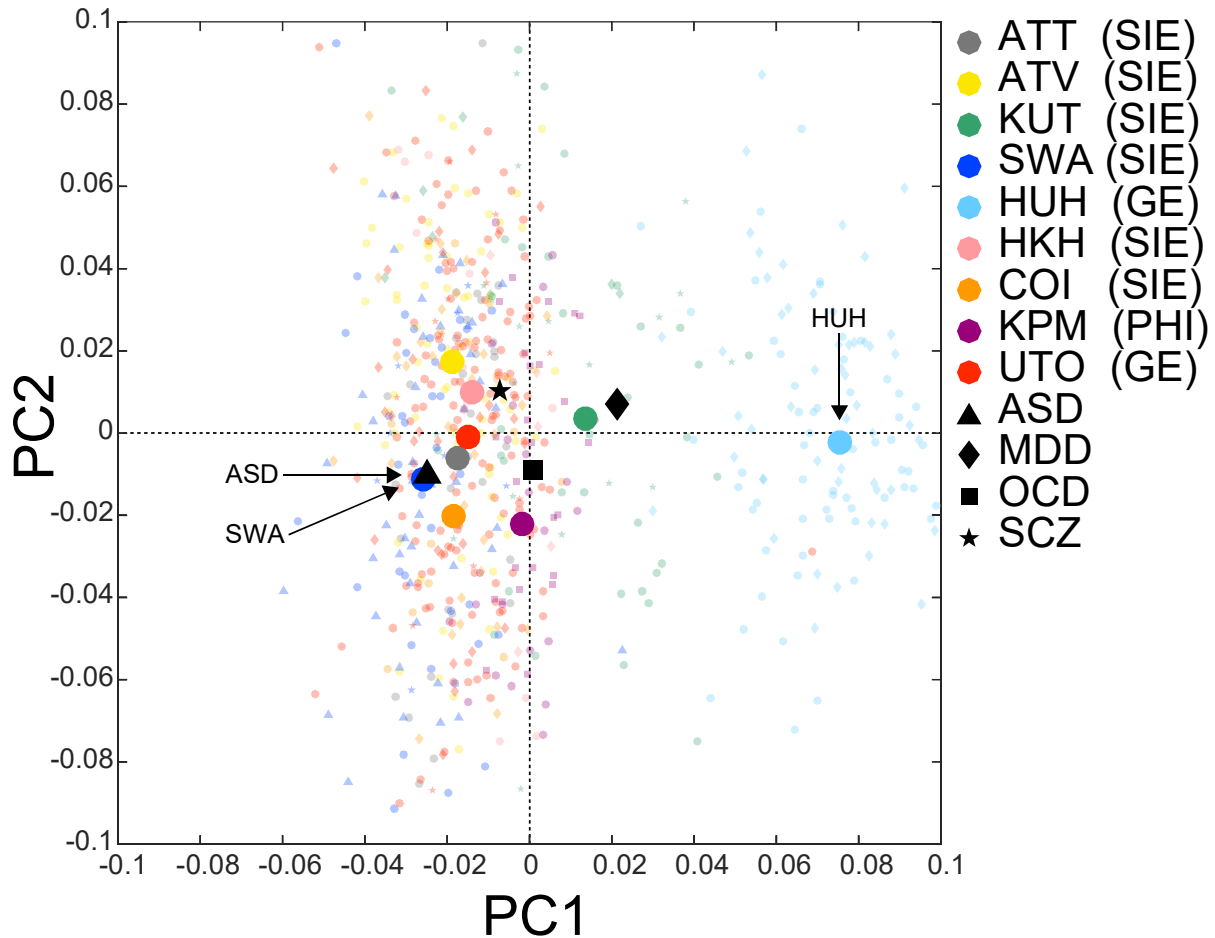
214

215

216 **Visualization of site differences and disorder effects**

217 We first visualized the site differences and disorder effects in the SRPBS multi-disorder rs-
218 fcMRI dataset while maintaining its quantitative properties by using a principal component
219 analysis (PCA)—an unsupervised dimension reduction method. Functional connectivity was
220 calculated as the temporal correlation of rs-fMRI blood-oxygen-level dependent (BOLD)
221 signals between two brain regions for each participant. There are some candidates for the
222 measure of functional connectivity such as the tangent method and partial correlation [11, 23];
223 however, we used Pearson's correlation coefficients because they have been the most
224 commonly used values in previous studies. Functional connectivity was defined based on a
225 functional brain atlas consisting of 268 nodes (i.e., regions) covering the whole brain, which
226 has been widely utilized in previous studies [20, 24-26]. The Fisher's z -transformed Pearson's
227 correlation coefficients between the preprocessed BOLD signal time courses of each possible
228 pair of nodes were calculated and used to construct 268×268 symmetrical connectivity
229 matrices in which each element represents a connection strength, or edge, between two nodes.
230 We used 35,778 connectivity values [i.e., $(268 \times 267)/2$] of the lower triangular matrix of the
231 connectivity matrix. All participant data in the SRPBS multi-disorder dataset were plotted on
232 two axes consisting of the first two principal components (Fig. 2, small, light-colored symbols).
233 The averages of the HCs within individual sites and the averages of individual psychiatric or
234 developmental disorders are presented as dark-colored symbols in Fig. 2. There was a clear
235 separation of the Hiroshima University Hospital (HUH) site for principal component 1, which
236 explained most of the variance in the data. Furthermore, there were no differences between the
237 differences of the sites and the disorder factors. Patients with ASD were only scanned at the
238 Showa University (SWA) site; therefore, the averages for patients with ASD (\blacktriangle) and HCs
239 (blue \bullet) scanned at this site were projected to nearly identical positions (Fig. 2).

Raw data



240

241 **Figure 2: PCA dimension reduction in the SRPBS multi-disorder dataset.**

242 All participants in the SRPBS multi-disorder dataset projected into the first two principal
243 components (PCs), as indicated by small, light-colored markers. The average across all healthy
244 controls in each site and the average within each psychiatric disorder are depicted as dark-
245 colored makers. The color of the marker represents the site, while the shape represents the
246 psychiatric disorder. PCA: principal component analysis; SRPBS: Strategic Research Program
247 for Brain Sciences; ATT: Siemens TimTrio scanner at Advanced Telecommunications
248 Research Institute International; ATV: Siemens Verio scanner at Advanced
249 Telecommunications Research Institute International; KUT: Siemens TimTrio scanner at
250 Kyoto University; SWA: Showa University; HUH: Hiroshima University Hospital; HKH:
251 Hiroshima Kajikawa Hospital; COI: Center of Innovation in Hiroshima University; KPM:
252 Kyoto Prefectural University of Medicine; UTO: University of Tokyo; ASD: Autism Spectrum
253 Disorder. MDD: Major Depressive Disorder. OCD: Obsessive Compulsive Disorder. SCZ:
254 Schizophrenia. SIE: Siemens fMRI. GE: GE fMRI. PHI: Philips fMRI.

255

256

257 **Bias estimation**

258 To quantitatively investigate the site differences in the rs-fcMRI data, we identified
259 measurement biases, sampling biases, and disorder factors. We defined measurement bias for
260 each site as a deviation of the correlation value for each functional connection from its average
261 across all sites. We assumed that the sampling biases of the HCs and patients with psychiatric
262 disorders differed from one another. Therefore, we calculated the sampling biases for each site
263 separately for HCs and patients with each disorder. Disorder factors were defined as deviations
264 from the HC values. Sampling biases were estimated for patients with MDD and SCZ because
265 only these patients were sampled at multiple sites. Disorder factors were estimated for MDD,
266 SCZ, and ASD because patients with OCD were not scanned using the unified protocol.

267 It is difficult to separate site differences into measurement bias and sampling bias
268 using only the SRPBS multi-disorder dataset because the two types of bias covaried across
269 sites. Different samples (i.e., participants) were scanned using different parameters (i.e.,
270 scanners and imaging protocols). In contrast, the traveling-subject dataset included only
271 measurement bias because the participants were fixed. By combining the traveling-subject
272 dataset with the SRPBS multi-disorder dataset, we simultaneously estimated measurement bias
273 and sampling bias as different factors affected by different sites. We utilized a linear mixed-
274 effects model to assess the effects of both types of bias and disorder factors on functional
275 connectivity, as follows.

276

277 *Linear mixed-effects model for the SRPBS multi-disorder dataset*

278 In this model, the connectivity values of each participant in the SRPBS multi-disorder dataset
279 were composed of fixed and random effects. Fixed effects included the sum of the average
280 correlation values across all participants and all sites at baseline, the measurement bias, the
281 sampling bias, and the disorder factors. The combined effect of participant factors (i.e.,
282 individual difference) and scan-to-scan variations was regarded as the random effect (see

283 “Estimation of biases and factors” in the Methods section).

284

285 *Linear mixed-effects model for the traveling-subject dataset*

286 In this model, the connectivity values of each participant for a specific scan in the traveling-
287 subject dataset were composed of fixed and random effects. Fixed effects included the sum of
288 the average correlation values across all participants and all sites, participant factors, and
289 measurement bias. Scan-to-scan variation was regarded as the random effect. For each
290 participant, we defined the participant factor as the deviation of connectivity values from the
291 average across all participants.

292 We estimated all biases and factors by simultaneously fitting the aforementioned two
293 regression models to the functional connectivity values of the two different datasets. For this
294 regression analysis, we used data from participants scanned using a unified imaging protocol
295 in the SRPBS multi-disorder dataset and from all participants in the traveling-subject dataset.
296 In summary, each bias or each factor was estimated as a vector that included a dimension
297 reflecting the number of connectivity values (i.e., 35,778). Vectors included in our further
298 analyses are those for measurement bias at 12 sites, sampling bias of HCs at six sites, sampling
299 bias for patients with MDD at three sites, sampling bias for patients with SCZ at three sites,
300 participant factors of nine traveling-subjects, and disorder factors for MDD, SCZ, and ASD.

301

302 **Quantification of site differences**

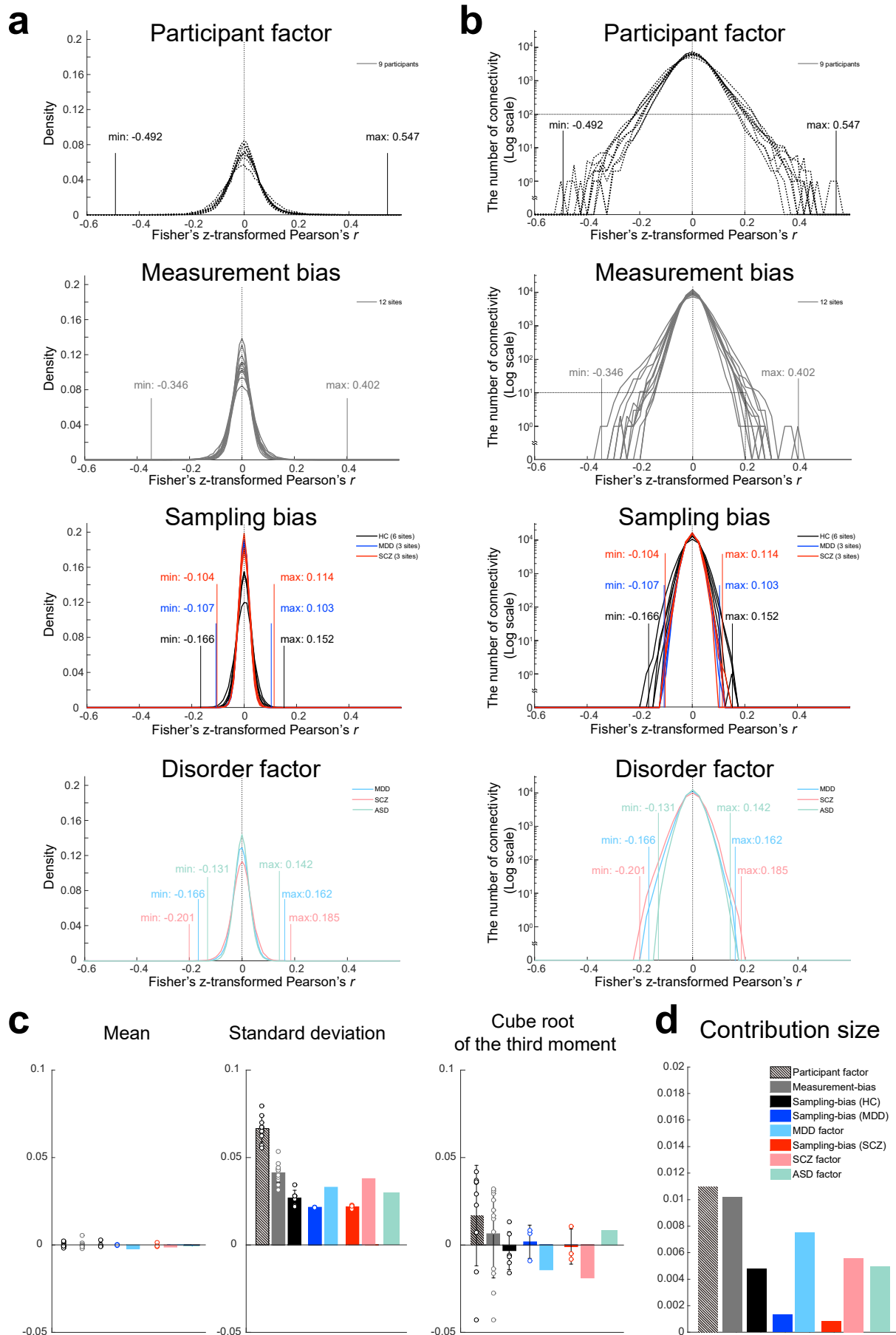
303 To quantitatively evaluate the effect of measurement and sampling biases on functional
304 connectivity, we compared the magnitudes of both types of bias with the magnitudes of
305 psychiatric disorders and participant factors. For this purpose, we investigated the magnitude
306 distribution of both biases, as well as the effects of psychiatric disorders and participant factors
307 on functional connectivity overall 35,778 elements in a 35,778-dimensional vector to see how
308 many functional connectivities were largely affected (Fig. 3a: the *x*-axis shows the magnitude

309 as Fisher's z -transformed Pearson's correlation coefficients, while the y -axis shows the density
310 of the number of connectivities). Figure 3b shows the same data, except the y -axis represents
311 the log-transformed number of connectivities for better visualization of small values. These
312 distributions show that, on average, connectivity was unaffected by either type of bias or by
313 each factor because the averages of each distribution were nearly 0. However, there were
314 significant differences among biases and factors for larger magnitudes near the tails of their
315 distributions. For example, the number of connectivities, which was largely affected (i.e., a
316 magnitude larger than 0.2), was more than 100 for the participant factor, approximately 100
317 for measurement bias, and nearly 0 for all sampling biases, as well as all disorder factors.

318 To quantitatively summarize the effect of each factor, we calculated the first, second,
319 and third statistical moments of each histogram (Fig. 3c). Based on the mean values and the
320 cube roots of the third moments, all distributions could be approximated as bilaterally
321 symmetric with a mean of zero. Thus, distributions with larger squared roots of the second
322 moments (standard deviations) affect more connectivities with larger effect sizes. The value
323 of the standard deviation was largest for the participant factor (0.0662), followed by these
324 values for the measurement bias (0.0411), the SCZ factor (0.0377), the MDD factor (0.0328),
325 the ASD factor (0.0297), the sampling bias for HCs (0.0267), sampling bias for patients with
326 SCZ (0.0217), and sampling bias for patients with MDD (0.0214). To compare the sizes of
327 the standard deviation between participant factors and measurement bias, we evaluated the
328 variance of each distribution. All pairs of variances were analyzed using Ansari–Bradley tests.
329 Our findings indicated that all variances of the participant factors were significantly larger
330 than all variances of the measurement biases (nine participant factors \times 12 measurement
331 biases = 108 pairs; W^* : mean = -59.80, max = -116.81, min = -3.69; p value after Bonferroni
332 correction: max = 0.011, min = 0, $n = 35,778$). In addition, the variances of 10 of 12
333 measurement biases were significantly larger than the variance of the MDD factor, the
334 variances of seven of 12 measurement biases were significantly larger than the variance of

335 the SCZ factor, and the variances of all measurement biases were significantly larger than the
336 variance of the MDD factor (Supplementary Table 8). Furthermore, we plotted fractions of
337 the data variance determined using the aforementioned factors (i.e., contribution size) in our
338 linear mixed-effects model (Fig. 3d; see “Analysis of contribution size” in the Methods
339 section). The results were consistent with the analysis of the standard deviation (Fig. 3c,
340 middle). These results indicate that the effect size of measurement bias on functional
341 connectivity is smaller than that of the participant factor but is mostly larger than those of the
342 disorder factors, which suggest that measurement bias represents a serious limitation in
343 research regarding psychiatric disorders. The largest variance in sampling bias was
344 significantly larger than the variance of the MDD factor (Supplementary Table 9), whereas
345 the smallest variance in sampling bias was one-half the size of the variance for disorder factors.
346 These findings indicate that sampling bias also represents a major limitation in psychiatric
347 research.

348 The standard deviation of the participant factor was approximately twice that for SCZ,
349 MDD, and ASD; therefore, individual variability within the healthy population was much
350 greater than that among patients with SCZ, MDD, or ASD when all functional connections
351 were considered. Furthermore, the standard deviations of the measurement biases were mostly
352 larger than those of the disorder factors, while the standard deviations of the sampling biases
353 were comparable with those of the disorder factors. Such relationships make the development
354 of rs-fcMRI-based classifiers of psychiatric or developmental disorders very challenging.
355 Only when a small number of disorder-specific and site-independent abnormal functional
356 connections can be selected from among a vast number does it become feasible to develop
357 robust and generalizable classifiers across multiple sites [2, 8-10, 15].



358

359

Figure 3: Distributions and statistics for each type of bias and each factor.

360 (a, b) The distribution of the effects of each bias and each factor on functional connectivity
361 vectors. Functional connectivity was measured based on Fisher's z-transformed Pearson's
362 correlation coefficients. The *x*-axis represents the effect size of the Fisher's z-transformed
363 Pearson's correlation coefficients. In (a) and (b), the *y*-axis represents the density of
364 connectivity and the log-transformed the number of connections, respectively. Each line
365 represents one participant or one site. (c) The means, standard deviations, and third moments
366 standardized to the same scale on the vertical axis (i.e., cube root) for each type of bias and
367 each factor. Bars represent the average value, while the error bars represent the standard
368 deviation across sites or participants. Each data point represents one participant or one site. (d)
369 Contribution size of each bias and each factor. HC: healthy controls; SCZ: schizophrenia;
370 MDD: major depressive disorder; ASD: autism spectrum disorder.

371

372 **Brain regions contributing most to biases and associated factors**

373 To evaluate the spatial distribution of the two types of bias and all factors in the whole brain,
374 we utilized a previously described visualization method [27] to project connectivity
375 information to anatomical regions of interest (ROIs). We first quantified the effect of a bias or
376 a factor on each functional connectivity as the median of its absolute values across sites or
377 across participants. Thus, we obtained 35,778 values, each of which was associated with one
378 connectivity and represented the effect of a bias or factor on the connectivity. We then
379 summarized these effects on connectivity for each ROI by averaging the values of all
380 connectivities connected with the ROI (see "Spatial characteristics of measurement bias,
381 sampling bias, and each factor in the brain" in the Methods section). The average value
382 represents the extent the ROI contributes to the effect of a bias or factor. By repeating this
383 procedure for each ROI and coding the averaged value based on the color of an ROI, we were
384 able to visualize the relative contribution of individual ROIs to each bias or factor in the whole
385 brain (Fig. 4). Consistent with the findings of previous studies, the effect of the participant
386 factor was large for several ROIs in the cerebral cortex, especially in the prefrontal cortex, but
387 small in the cerebellum and visual cortex [24]. The effect of measurement bias was large in
388 inferior brain regions where functional images are differentially distorted depending on the
389 phase-encoding direction [28, 29]. Connections involving the medial dorsal nucleus of the

390 thalamus were also heavily affected by both MDD, SCZ and ASD. Effects of the MDD factor
391 were observed in the dorsomedial prefrontal cortex and the superior temporal gyrus in which
392 abnormalities have also been reported in previous studies [22, 30, 31]. Effects of the SCZ factor
393 were observed in the left inferior parietal lobule, bilateral anterior cingulate cortices, and left
394 middle frontal gyrus in which abnormalities have been reported in previous studies [32-34].
395 Effects of the ASD factor were observed in the putamen, the medial prefrontal cortex, and the
396 right middle temporal gyrus in which abnormalities have also been reported in previous studies
397 [10, 11, 35]. The effect of sampling bias for HCs was large in the inferior parietal lobule and
398 the precuneus, both of which are involved in the default mode network and the middle frontal
399 gyrus. Sampling bias for disorders was large in the medial dorsal nucleus of the thalamus, left
400 dorsolateral prefrontal cortex, dorsomedial prefrontal cortex, and cerebellum for MDD [22];
401 and in the prefrontal cortex, cuneus, and cerebellum for SCZ [33].

402

403

404

405

406

407

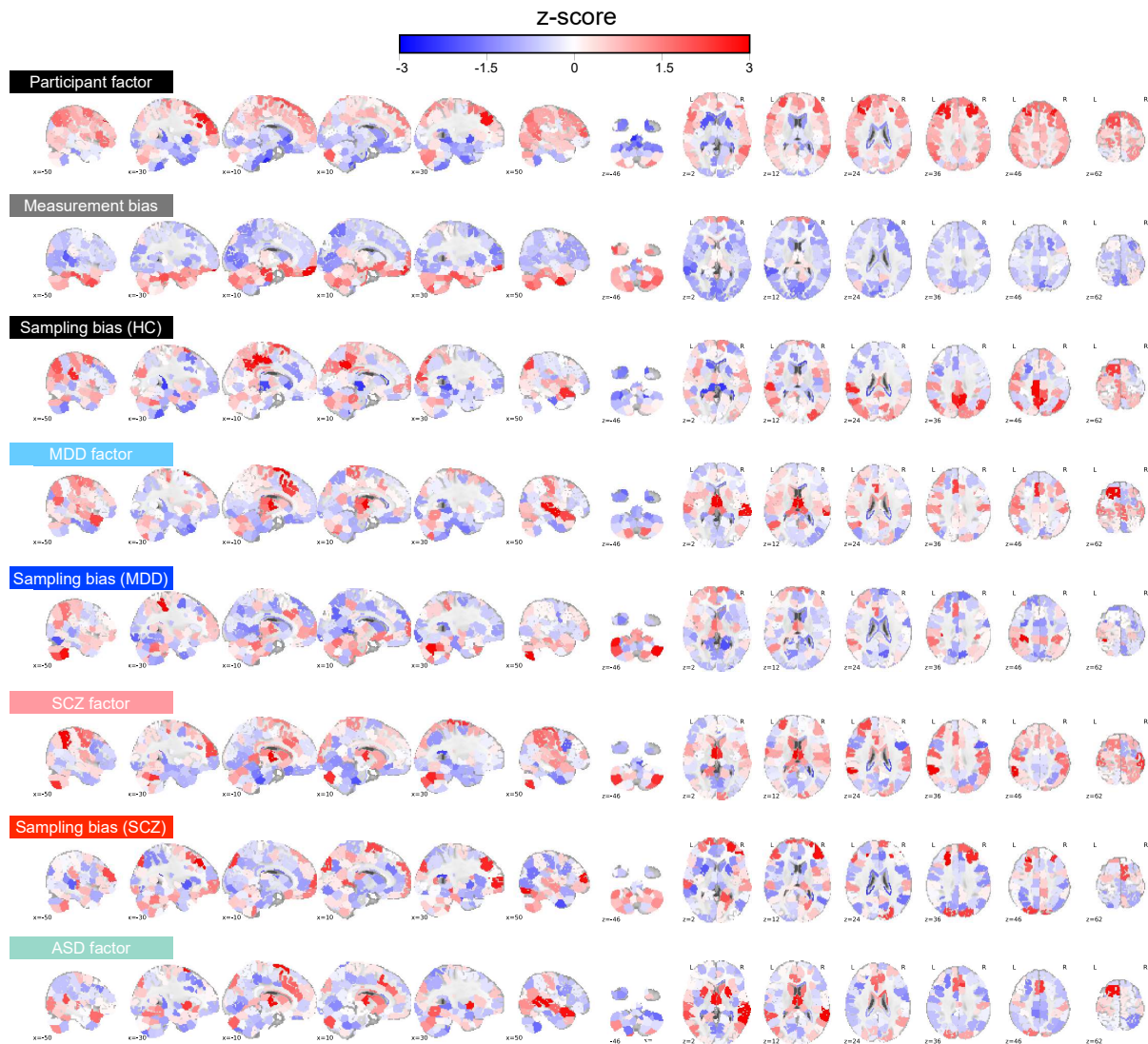
408

409

410

411

412



413

414 **Figure 4: Spatial distribution of each type of bias and each factor in various brain regions.**

415 Mean effects of connectivity for all 268 ROIs. For each ROI, the mean effects of all functional
416 connections associated with that ROI were calculated for each bias and each factor. Warmer
417 (red) and cooler (blue) colors correspond to large and small effects, respectively. The
418 magnitudes of the effects are normalized within each bias or each factor (z-score). ROI: region
419 of interest; HC: healthy control; SCZ: schizophrenia; MDD: major depressive disorder; ASD:
420 autism spectrum disorder.

421

422

423

424

425

426

427 **Characteristics of measurement bias**

428 We next investigated the characteristics of measurement bias. We first examined whether
429 similarities among the estimated measurement bias vectors for the 12 included sites reflect
430 certain properties of MRI scanners such as phase-encoding direction, MRI manufacturer, coil
431 type, and scanner type. We used hierarchical clustering analysis to discover clusters of similar
432 patterns for measurement bias. This method has previously been used to distinguish subtypes
433 of MDD, based on rs-fcMRI data [22]. As a result, the measurement biases of the 12 sites were
434 divided into phase-encoding direction clusters at the first level (Fig. 5a). They were divided
435 into fMRI manufacturer clusters at the second level, and further divided into coil type clusters,
436 followed by scanner model clusters. Furthermore, we quantitatively verified the magnitude
437 relationship among factors by using the same model to assess the contribution of each factor
438 (Fig. 5b; see “Analysis of contribution size” in the Methods section). The contribution size was
439 largest for the phase-encoding direction (0.0391), followed by the contribution sized for fMRI
440 manufacturer (0.0318), coil type (0.0239), and scanner model (0.0152). These findings indicate
441 that the main factor influencing measurement bias is the difference in the phase-encoding
442 direction, followed by fMRI manufacturer, coil type, and scanner model, respectively.

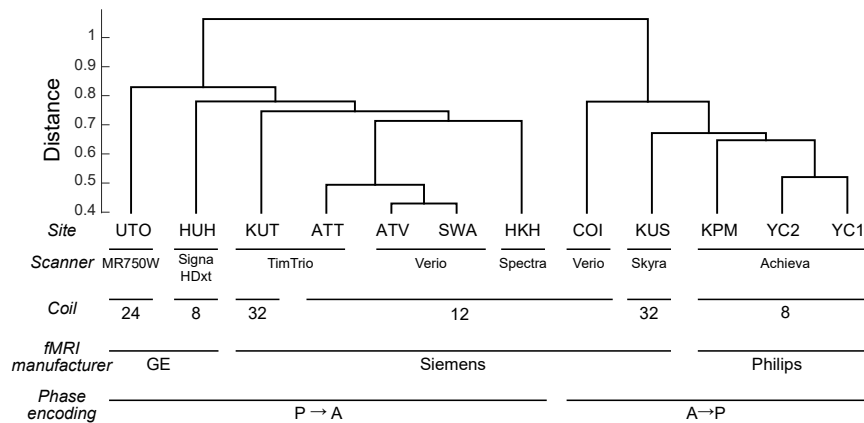
443

444

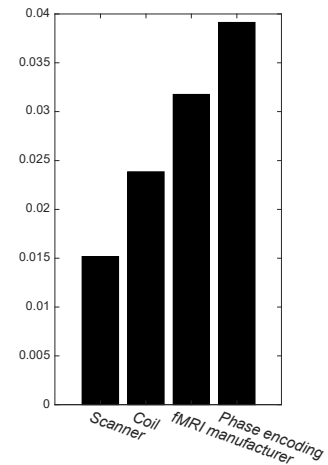
445

446

a Clustering dendrogram



b Contribution size



447

448 **Figure 5: Clustering dendrogram for measurement bias.**

449 (a) The height of each linkage in the dendrogram represents the dissimilarity ($1 - r$) between
 450 the clusters joined by that link. (b) Contribution size of each factor. UTO: University of Tokyo;
 451 HUH: Hiroshima University Hospital; KUT: Siemens TimTrio scanner at Kyoto University;
 452 ATT: Siemens TimTrio scanner at Advanced Telecommunications Research Institute
 453 International; ATV: Siemens Verio scanner at Advanced Telecommunications Research
 454 Institute International; SWA: Showa University; HKH: Hiroshima Kajikawa Hospital; COI:
 455 Center of Innovation in Hiroshima University; KUS: Siemens Skyra scanner at Kyoto
 456 University; KPM: Kyoto Prefectural University of Medicine; YC1: Yaesu Clinic 1; YC2:
 457 Yaesu Clinic 2.

458

459

460

461

462

463

464

465

466

467

468

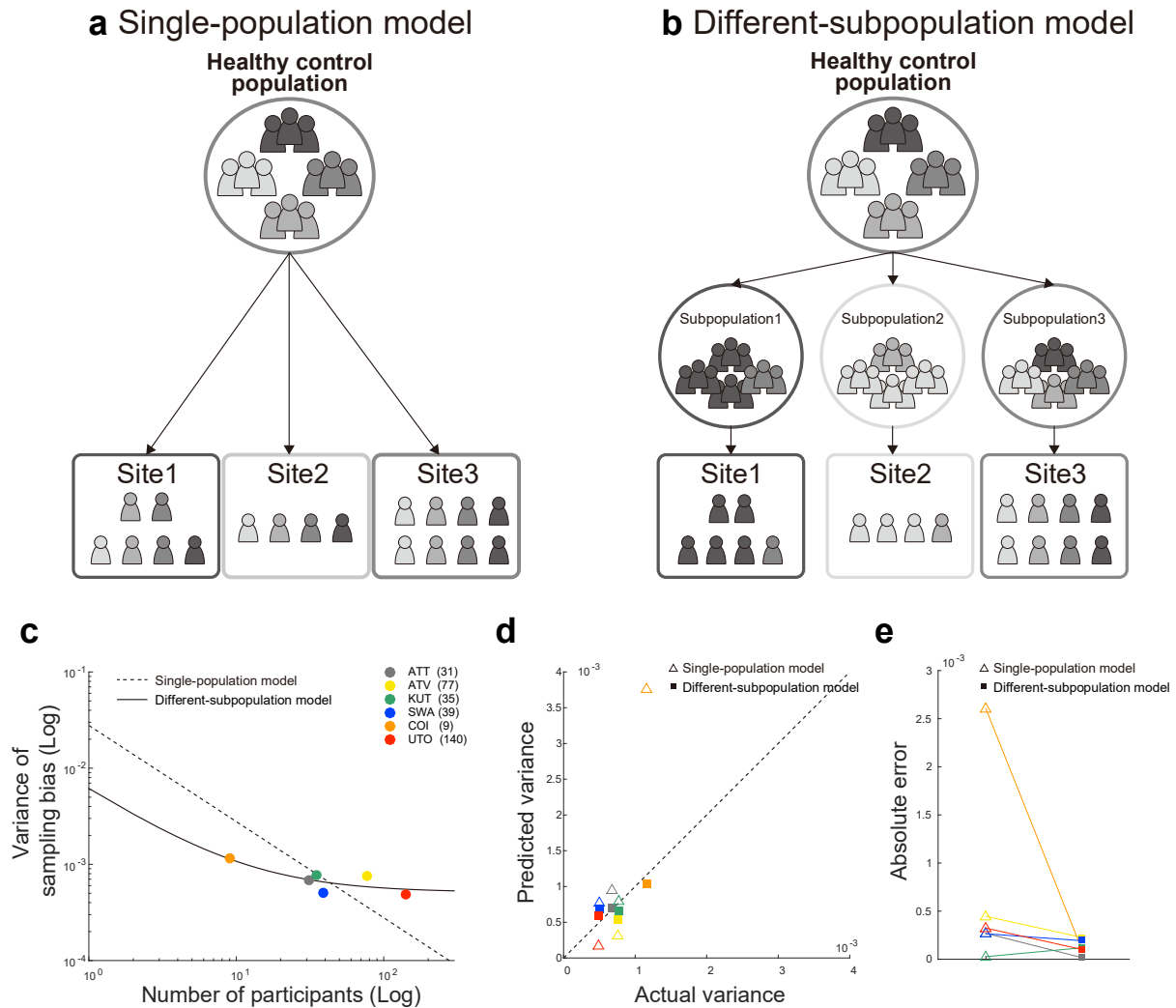
469

470 **Sampling bias is because of sampling from among a subpopulation**

471 We investigated two alternative models for the mechanisms underlying sampling bias. In the
472 “single-population model”, which assumes that participants are sampled from a common
473 population (Fig. 6a), the functional connectivity values of each participant were generated from
474 a Gaussian distribution (see “Comparison of models for sampling bias” in the Methods section).
475 In the “different-subpopulation model,” which assumes that sampling bias occurs partly
476 because participants are sampled from among a different subpopulation at each site (Fig. 6b),
477 we assumed that the average of the subpopulation differed among sites and was generated from
478 a Gaussian distribution. In addition, the functional connectivity values of each participant were
479 generated from a Gaussian distribution, based on the average of the subpopulation at each site.
480 It is necessary to determine which model is more suitable for collecting big data across multiple
481 sites: If the former model is correct, then the data can be used to represent a population by
482 increasing the number of participants, even if the number of sites is small. If the latter model
483 is correct, data should be collected from many sites, as a single site does not represent the true
484 grand population distribution, even with a very large sample size.

485 For each model, we first investigated how the number of participants at each site
486 determined the effect of sampling bias on functional connectivity. We measured the magnitude
487 of the effect, based on the variance values for sampling bias across functional connectivity (see
488 the “Quantification of site differences” section). We used variance instead of the standard
489 deviation to simplify the statistical analysis, although there is essentially no difference based
490 on which value is used. We theorized that each model represents a different relationship
491 between the number of participants and the variance of sampling bias. Therefore, we
492 investigated which model best represents the actual relationships in our data by comparing the
493 corrected Akaike information criterion (AICc) [36, 37] and Bayesian information criterion
494 (BIC). Moreover, we performed leave-one-site-out cross-validation evaluations of predictive
495 performance in which all but one site was used to construct the model and the variance of the

496 sampling bias was predicted for the remaining site. We then compared the predictive
497 performances between the two models. Our results indicated that the different-subpopulation
498 model provided a better fit for our data than the single-population model (Fig. 6c; different-
499 subpopulation model: AICc = -108.80 and BIC = -113.22; single-population model: AICc = -
500 96.71 and BIC = -97.92). Furthermore, the predictive performance was significantly higher for
501 the different-subpopulation model than for the single-population model (one-tailed Wilcoxon
502 signed-rank test applied to absolute errors: $Z = 1.67$, $p = .0469$, $n = 6$; Figs. 6d and 6e). This
503 result indicates that sampling bias is not only caused by random sampling from a single grand
504 population, depending on the number of participants among sites, but also by sampling from
505 among different subpopulations. Sampling biases thus represent a major limitation in
506 attempting to estimate a true single distribution of HC or patient data based on measurements
507 obtained from a finite number of sites and participants.



508

509

Figure 6: Comparison of the two models of sampling bias.

510

Schematic examples illustrating the single-population (a) and different-subpopulation models

511

(b) and the results of model fitting (c). The *x*-axis represents the number of participants on a

512

logarithmic scale, while the *y*-axis represents the variance of sampling bias on a logarithmic

513

scale. The broken line represents the prediction of the single-population model, while the solid

514

line represents the prediction of the different-subpopulation model. Each data point represents

515

one site. (d) Results of the predictions determined by using each model. The *x*-axis represents

516

the actual variance, while the *y*-axis represents the predicted variance. Open triangles

517

correspond to the single-population model, while filled squares correspond to the different-

518

subpopulation model. (e) Performance of prediction using the two models, based on the

519

absolute error between the actual and predicted variance. UTO: University of Tokyo; COI:

520

Center of Innovation in Hiroshima University; SWA: Showa University; KUT: Siemens

521

TimTrio scanner at Kyoto University; ATT: Siemens TimTrio scanner at Advanced

522

Telecommunications Research Institute International; ATV: Siemens Verio scanner at

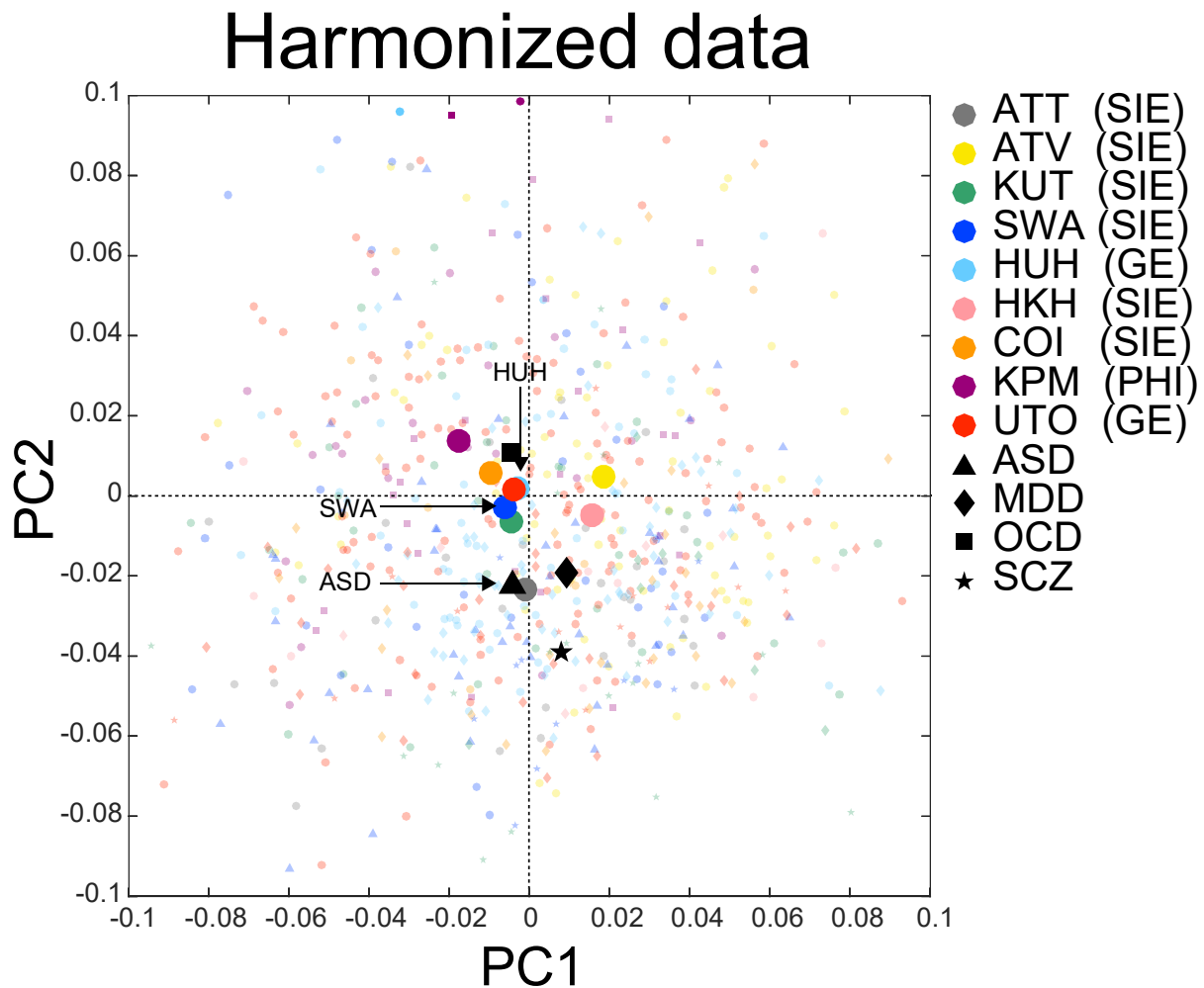
523

Advanced Telecommunications Research Institute International.

524

525 **Visualization of the effect of harmonization**

526 We next developed a novel harmonization method that enabled us to subtract only the
527 measurement bias using the traveling-subject dataset. Using a linear mixed-effects model, we
528 estimated the measurement bias separately from sampling bias (see the “Bias estimation” in
529 the Methods section). Thus, we could remove the measurement bias from the SRPBS multi-
530 disorder dataset (i.e., traveling-subject method, see “Traveling-subject harmonization” in the
531 Methods section). To visualize the effects of the harmonization process, we plotted the data
532 after subtracting only the measurement bias from the SRPBS multi-disorder dataset as
533 described in the “Visualization of site differences and disorder effects” section (Fig. 7).
534 Relative to the data reported in Fig. 2, which reflects the data before harmonization, the HUH
535 site moved much closer to the origin (i.e., grand average) and showed no marked separation
536 from the other sites. This result indicates that the separation of the HUH site observed in Fig.
537 2 was caused by measurement bias, which was removed following harmonization. Furthermore,
538 harmonization was effective in distinguishing patients and HCs scanned at the same site. Since
539 patients with ASD were only scanned at the Showa University (SWA) site, the averages for
540 patients with ASD (▲) and HCs (blue ●) scanned at this site were projected to nearly identical
541 positions (Fig. 2). However, the two symbols are clearly separated from one another in Fig. 7.
542 The effect of a psychiatric disorder (ASD) could not be observed in the first two PCs without
543 harmonization but became detectable following the removal of measurement bias.



544

545 **Figure 7: PCA dimension reduction in the SRPBS multi-disorder dataset after**
546 **harmonization.**

547 All participants in the SRPBS multi-disorder dataset after harmonization projected into the first
548 two principal components (PCs), as indicated by small, light-colored markers. The average
549 across all healthy controls in each site and the average within each psychiatric disorder are
550 depicted as dark-colored markers. The color of the marker represents the site, while the shape
551 represents the psychiatric disorder. PCA: principal component analysis; SRPBS: Strategic
552 Research Program for Brain Sciences; ATT: Siemens TimTrio scanner at Advanced
553 Telecommunications Research Institute International; ATV: Siemens Verio scanner at
554 Advanced Telecommunications Research Institute International; KUT: Siemens TimTrio
555 scanner at Kyoto University; SWA: Showa University; HUH: Hiroshima University Hospital;
556 HKH: Hiroshima Kajikawa Hospital; COI: Center of Innovation in Hiroshima University;
557 KPM: Kyoto Prefectural University of Medicine; UTO: University of Tokyo; ASD: Autism
558 Spectrum Disorder. MDD: Major Depressive Disorder. OCD: Obsessive Compulsive Disorder.
559 SCZ: Schizophrenia. SIE: Siemens fMRI. GE: GE fMRI. PHI: Philips fMRI.

560

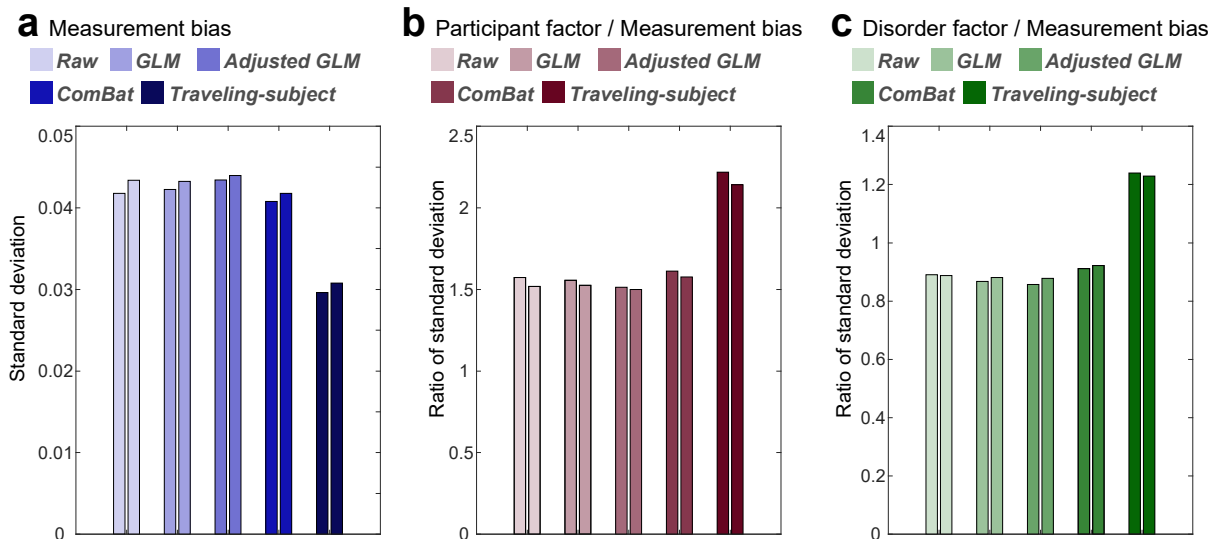
561 **Quantification of the effect of traveling-subject harmonization**

562 To correct difference among sites there are three commonly used harmonization methods: (1)
563 a ComBat method [16, 17, 19, 38], a batch-effect correction tool commonly used in genomics,
564 site difference was modeled and removed; (2) a generalized linear model (GLM) method, site
565 difference was estimated without adjusting for biological covariates (e.g., diagnosis) [16, 18,
566 22]; and (3) an adjusted GLM method, site difference was estimated while adjusting for
567 biological covariates [16, 18] (see the “Harmonization procedures” in the Methods section).
568 However, all these methods estimate the site difference without separating site difference into
569 the measurement bias and the sampling bias and subtract the site difference from data.
570 Therefore, existing harmonization methods might have pitfall to eliminate not only biologically
571 meaningless measurement bias but also eliminate biologically meaningful sampling bias. Here,
572 we tested whether the traveling-subject harmonization method indeed removes only the
573 measurement bias and whether the existing harmonization methods simultaneously remove the
574 measurement and sampling biases. Specifically, we performed 2-fold cross-validation
575 evaluations in which the SRPBS multi-disorder dataset was partitioned into two equal-size
576 subsamples (fold1 data and fold2 data) with the same proportions of sites. Between these two
577 subsamples, the measurement bias is common, but the sampling bias is different (because the
578 scanners are common, and participants are different). We estimated the measurement bias (or
579 site difference including the measurement bias and the sampling bias for the existing methods)
580 by applying the harmonization methods to the fold1 data and subtracted the measurement bias
581 or site difference from the fold2 data. We then estimated the measurement bias in the fold2
582 data. For the existing harmonization methods, if the site difference estimated by using fold1
583 contains only the measurement bias, the measurement bias estimated in fold2 data after
584 subtracting the site difference should be smaller than that of without subtracting the site
585 difference (Raw). To separately estimate measurement bias and sampling bias in both
586 subsamples while avoiding information leak, we also divided the traveling-subject dataset into

587 two equal-size subsamples with the same proportions of sites and subjects. We concatenated
588 one subsample of traveling-subject dataset to fold1 data to estimate the measurement bias for
589 traveling-subject method (estimating dataset) and concatenated the other subsample of
590 traveling-subject dataset to fold2 data for testing (testing dataset). That is, in the traveling-
591 subject harmonization method, we estimated the measurement bias using the estimating dataset
592 and removed the measurement bias from the testing dataset. By contrast, in the other
593 harmonization methods, we estimated the site difference using the fold1 data (not including the
594 subsample of traveling-subject dataset) and removed the site difference from the testing dataset.
595 We then estimated the measurement bias using the testing dataset and evaluated the standard
596 deviation of the magnitude distribution of measurement bias calculated in the same way as
597 described in “Quantification of site differences” section. To verify whether important
598 information such as participant factors and disorder factors are kept in the testing dataset, we
599 also estimated the disorder factors and participant factors and calculated the ratio of the
600 standard deviation of measurement bias to the standard deviation of participant factor and
601 disorder factor as signal to noise ratios. This procedure was done again by exchanging the
602 estimating dataset and the testing dataset (see the “2-fold cross-validation evaluation procedure”
603 in the Methods section).

604 Fig. 8 shows that the standard deviation of measurement bias and the ratio of the
605 standard deviation of measurement bias to the standard deviation of participant factor and
606 disorder factor in the both fold data for the four harmonization methods and without
607 harmonization (Raw). Our result shows that the reduction of the standard deviation of
608 measurement bias from the Raw was highest in the traveling-subject method among all
609 methods (29% reduction compared to 3% in the second highest value for ComBat method).
610 Moreover, improvement in the signal to noise ratios were also highest in our method for
611 participant factor (41% improvement compared to 3% in the second highest value for ComBat
612 method) and for disorder factor (39% improvement compared to 3% in the second highest value

613 for ComBat method). These results indicate that the traveling-subject harmonization method
614 indeed removed the measurement bias and improved the signal to noise ratios.
615



616
617 **Figure 8: Reduction of the measurement bias and improvement of signal to noise ratios**
618 **for different harmonization methods.**

619 (a) Standard deviation of the measurement bias. (b) Ratio of standard deviation of the
620 measurement bias to standard deviation of the participant factor. (c) Ratio of standard deviation
621 of the measurement bias to standard deviation of the disorder factor. Different colored columns
622 show the results from different harmonization method. Two columns of the same color show
623 the results of the two folds. GLM: generalized linear model.

624

625

626

627

628

629

630

631

632

633

634 **Discussion**

635 In the present study, by acquiring a separate traveling-subject dataset and the SRPBS multi-
636 disorder dataset, we separately estimated measurement and sampling biases for multiple sites,
637 which we then compared with the magnitude of disorder factors. Furthermore, we investigated
638 the origin of each bias in multi-site datasets. Finally, to overcome the problem of site difference,
639 we developed a novel harmonization method that enabled us to subtract the measurement bias
640 by using a traveling-subject dataset and achieved the reduction of the measurement bias by
641 29% and the improvement of the signal to noise ratios by 40%.

642 We assessed the effect sizes of measurement and sampling biases in comparison with
643 the effects of psychiatric disorders on resting-state functional connectivity. Our findings
644 indicated that measurement bias exerted significantly greater effects than disorder factors,
645 whereas sampling bias was comparable to (or even larger than) the disorder effects (Fig. 3).
646 However, we did not control for variations in disease stage and treatment in our dataset.
647 Although controlling for such heterogeneity may increase the effect size of disorder factors,
648 such control is not feasible when collecting big data from multiple sites. Therefore, it is
649 important to appropriately remove measurement bias from heterogeneous patient data to
650 identify relatively small disorder effects. This issue is essential for investigating the
651 relationships among different psychiatric disorders because disease factors are often
652 confounded by site differences. As previously mentioned, it is common for a single site to
653 sample only a few types of psychiatric disorders (e.g., SCZ from site A and ASD from site B).
654 In this situation, it is critical to dissociate disease factors from site differences. This dissociation
655 can be accomplished by subtracting only the measurement bias which is estimated from
656 traveling subject dataset.

657 Our results indicated that measurement bias is primarily influenced by differences in
658 the phase-encoding direction, followed by differences in fMRI manufacturer, coil type, and
659 scanner model (Fig. 5). These results are consistent with our finding of large measurement

660 biases in the inferior brain regions (Fig. 4), the functional imaging of which is known to be
661 influenced by the phase-encoding direction [28, 29]. Previous studies have reported that the
662 effect because of the difference in the phase-encoding direction can be corrected using the field
663 map obtained at the time of imaging [28, 39-41]. The field map was acquired in parts of the
664 traveling-subject dataset; therefore, we investigated the effectiveness of field map correction
665 by comparing the effect size of the measurement bias and the participant factor between
666 functional images with and without field map correction. Our prediction was as follows: if field
667 map correction is effective, the effect of measurement bias will decrease, while that of the
668 participant factor will increase following field map correction. Field map correction using
669 SPM12 (<http://www.fil.ion.ucl.ac.uk/spm/software/spm12>) reduced the effect of measurement
670 bias in the inferior brain regions (whole brain: 3% reduction in the standard deviation of
671 measurement bias) and increased the effect of the participant factor in the whole brain (3%
672 increase in the standard deviation of the participant factor; Supplementary Figures 2a and 2b).
673 However, the effect of measurement bias remained large in inferior brain regions
674 (Supplementary Figure 2a), and hierarchical clustering analysis revealed that the clusters of the
675 phase-encoding direction remained dominant (Supplementary Figure 2c). These results
676 indicate that, even with field map correction, it is largely impossible to remove the influence
677 of differences in phase-encoding direction on functional connectivity. Thus, harmonization
678 methods are still necessary to remove the effect of these differences and other measurement-
679 related factors. However, some distortion correction methods have been developed (e.g., top-
680 up method and symmetric normalization) [42, 43], and further studies are required to verify the
681 efficacy of these methods.

682 Our data supported the different-subpopulation model rather than the single-
683 population model (Fig. 6), which indicates that sampling bias is caused by sampling from
684 among different subpopulations. Furthermore, these findings suggest that, during big data
685 collection, it is better to sample participants from several imaging sites than to sample many

686 participants from a few imaging sites. These results were obtained only by combining the
687 SRPBS multi-disorder database with a traveling-subject dataset
688 (<http://www.cns.atr.jp/decnefpro/>). To the best of our knowledge, the present study is the first
689 to demonstrate the presence of sampling bias in rs-fcMRI data, the mechanisms underlying this
690 sampling bias, and the effect size of sampling bias on resting-state functional connectivity,
691 which was comparable to that of psychiatric disorders. We analyzed sampling bias among HCs
692 only, because the number of sites was too small to conduct an analysis of patients with
693 psychiatric diseases.

694 We developed a novel harmonization method using a traveling-subject dataset (i.e.,
695 traveling-subject method), which was then compared with existing harmonization methods.
696 Our results demonstrated that the traveling-subject method outperformed other conventional
697 GLM-based harmonization methods and ComBat method. The traveling-subject method
698 achieved reduction of the measurement bias by 29% compared to 3% in the second highest
699 value for ComBat method and improvement of the signal to noise ratios by 40% compared to
700 3% in the second highest value for ComBat method. This result indicates that the traveling-
701 subject dataset helps to properly estimate the measurement bias and also helps to harmonize
702 the rs-fMRI data across imaging sites. To further quantitatively evaluate the harmonization
703 method, we constructed biomarkers for psychiatric disorders based on rs-fcMRI data, which
704 distinguishes between HCs and patients, and a regression model to predict participants' age
705 based on rs-fcMRI data using SRPBS multi-disorder dataset (see “Classifiers for MDD and
706 SCZ, based on the four harmonization methods” and “Regression models of participant age
707 based on the four harmonization methods” in Supplementary Information). We evaluated the
708 generalization performance to independent validation dataset, which was not included in
709 SRPBS multi-disorder dataset. The traveling-subject harmonization method improved the
710 generalization performance of all these prediction models as compared with the case where
711 harmonization was not performed. These results indicate that the traveling-subject dataset also

712 helps the constructing a prediction model based on multi-site rs-fMRI data.

713 The present study possesses some limitations of note. The accuracy of measurement
714 bias estimation may be improved by further expanding the traveling-subject dataset. This can
715 be achieved by increasing the number of traveling participants or sessions per site. However,
716 as mentioned in a previous traveling-subject study [20], it is costly and time-consuming to
717 ensure that numerous participants travel to every site involved in big database projects. Thus,
718 the cost-performance tradeoff must be evaluated in practical settings. The numbers of traveling
719 participants and MRI sites used in this study (nine and 12, respectively) were larger than those
720 used in a previous study (eight and eight, respectively) [20], and the number of total sessions
721 in this study (411) was more than three times larger than that used in the previous study (128)
722 [20]. Furthermore, although we estimated the measurement bias for each connectivity,
723 hierarchical models of the brain (e.g., ComBat) may be more appropriate for improving the
724 estimates of measurement bias.

725 In summary, by acquiring a separate traveling-subject dataset and the SRPBS multi-
726 disorder database, we revealed that site differences were composed of biological sampling bias
727 and engineering measurement bias. The effect sizes of these biases on functional connectivity
728 were greater than or equal to the effect sizes of psychiatric disorders, highlighting the
729 importance of controlling for site differences when investigating psychiatric disorders.
730 Furthermore, using the traveling-subject dataset, we developed a novel traveling-subject
731 method that harmonizes the measurement bias only by separating sampling bias from site
732 differences. Our findings verified that the traveling-subject method outperformed conventional
733 GLM-based harmonization methods and ComBat method. These results suggest that a
734 traveling-subject dataset can help to harmonize the rs-fMRI data across imaging sites.

735

736

737

738 **Methods**

739 **Participants**

740 We used two resting-state functional MRI datasets for all analyses: (1) the SRPBS multi-disorder dataset, which encompasses
741 multiple psychiatric disorders; (2) a traveling-subject dataset. The SRPBS multi-disorder dataset contains data for 805
742 participants (482 HCs from nine sites, 161 patients with MDD from five sites, 49 patients with ASD from one site, 65 patients
743 with OCD from one site, and 48 patients with SCZ from three sites (Supplementary Table 1). Data were acquired using a
744 Siemens TimTrio scanner at Advanced Telecommunications Research Institute International (ATT), a Siemens Verio scanner
745 at Advanced Telecommunications Research Institute International (ATV), a Siemens Verio at the Center of Innovation in
746 Hiroshima University (COI), a GE Signa HDxt scanner at HUH, a Siemens Spectra scanner at Hiroshima Kajikawa Hospital
747 (HKH), a Philips Achieva scanner at Kyoto Prefectural University of Medicine (KPM), a Siemens Verio scanner at SWA, a
748 Siemens TimTrio scanner at Kyoto University (KUT), and a GE MR750W scanner at the University of Tokyo (UTO). Each
749 participant underwent a single rs-fMRI session for 5–10 min. The rs-fMRI data were acquired using a unified imaging protocol
750 at all but three sites (Supplementary Table 2; <http://www.cns.atr.jp/rs-fmri-protocol-2/>). During the rs-fMRI scans, participants
751 were instructed as follows, except at one site: “Please relax. Don’t sleep. Fixate on the central crosshair mark and do not think
752 about specific things.” At the remaining site, participants were instructed to close their eyes rather than fixate on a central
753 crosshair.

754 In the traveling-subject dataset, nine healthy participants (all male participants; age range, 24–32 years; mean age,
755 27 ± 2.6 years) were scanned at each of 12 sites in the SRPBS consortium, producing a total of 411 scan sessions. Data were
756 acquired at the sites included in the SRPBS multi-disorder database (i.e., ATT, ATV, COI, HUH, HKH, KPM, SWA, KUT,
757 and UTO) and three additional sites: Kyoto University (KUS; Siemens Skyra) and Yaesu Clinic 1 and 2 (YC1 and YC2; Philips
758 Achieva) (Supplementary Table 3). Each participant underwent three rs-fMRI sessions of 10 min each at nine sites, two
759 sessions of 10 min each at two sites (HKH & HUH), and five cycles (morning, afternoon, next day, next week, next month)
760 consisting of three 10-minute sessions each at a single site (ATT). In the latter situation, one participant underwent four rather
761 than five sessions at the ATT site because of a poor physical condition. Thus, a total of 411 sessions were conducted [8
762 $\text{participants} \times (3 \times 9 + 2 \times 2 + 5 \times 3 \times 1) + 1 \text{ participant} \times (3 \times 9 + 2 \times 2 + 4 \times 3 \times 1)$]. During each rs-fMRI session, participants were
763 instructed to maintain a focus on a fixation point at the center of a screen, remain still and awake, and to think about nothing
764 in particular. For sites that could not use a screen in conjunction with fMRI (HKH & KUS), a seal indicating the fixation point
765 was placed on the inside wall of the MRI gantry. Although we attempted to ensure imaging was performed using the same
766 parameters at all sites, there were two phase-encoding directions (P→A and A→P), three MRI manufacturers (Siemens, GE,
767 and Philips), four different numbers of coils (8, 12, 24, 32), and seven scanner types (TimTrio, Verio, Skyra, Spectra, MR750W,
768 SignaHDxt, Achieva) (Supplementary Table 3).

769 All participants in all datasets provided written informed consent, and all recruitment procedures and experimental
770 protocols were approved by the Institutional Review Boards of the principal investigators’ respective institutions (Advanced
771 Telecommunications Research Institute International (ATR), Hiroshima University, Kyoto Prefectural University of Medicine,
772 Showa University, The University of Tokyo).

773

774 **Preprocessing and calculation of the resting-state functional connectivity matrix**

775 The rs-fMRI data were preprocessed using SPM8 implemented in MATLAB. The first 10 s of data were discarded to allow

776 for T1 equilibration. Preprocessing steps included slice-timing correction, realignment, co-registration, segmentation of T1-
777 weighted structural images, normalization to Montreal Neurological Institute (MNI) space, and spatial smoothing with an
778 isotropic Gaussian kernel of 6 mm full-width at half-maximum. For the analysis of connectivity matrices, ROIs were delineated
779 according to a 268-node gray matter atlas developed to cluster maximally similar voxels [26]. The BOLD signal time courses
780 were extracted from these 268 ROIs. To remove several sources of spurious variance, we used linear regression with 36
781 regression parameters [44] such as six motion parameters, average signals over the whole brain, white matter, and cerebrospinal
782 fluid. Derivatives and quadratic terms were also included for all parameters. A temporal band-pass filter was applied to the
783 time series using a first-order Butterworth filter with a pass band between 0.01 Hz and 0.08 Hz to restrict the analysis to low-
784 frequency fluctuations, which are characteristic of rs-fMRI BOLD activity [44]. Furthermore, to reduce spurious changes in
785 functional connectivity because of head motion, we calculated frame-wise displacement (FD) and removed volumes with FD
786 > 0.5 mm, as proposed in a previous study [45]. The FD represents head motion between two consecutive volumes as a scalar
787 quantity (i.e., the summation of absolute displacements in translation and rotation). Using the aforementioned threshold, $5.4\% \pm 10.6\%$ volumes (i.e., the average [approximately 13 volumes] ± 1 SD) were removed per 10 min of rs-fMRI scanning (240
789 volumes) in the traveling-subject dataset, $6.2\% \pm 13.2\%$ volumes were removed per rs-fMRI session in the SRPBS multi-
790 disorder dataset. If the number of volumes removed after scrubbing exceeded the average of -3 SD across participants in each
791 dataset, the participants or sessions were excluded from the analysis. As a result, 14 sessions were removed from the traveling-
792 subject dataset, 20 participants were removed from the SRPBS multi-disorder dataset. Furthermore, we excluded participants
793 for whom we could not calculate functional connectivity at all 35,778 connections, primarily because of the lack of BOLD
794 signals within an ROI. As a result, 99 participants were further removed from the SRPBS multi-disorder dataset.

795

796 **Principal component analysis**

797 We developed bivariate scatter plots of the first two principal components based on a PCA of functional connectivity values
798 in the SRPBS multi-disorder dataset (Fig. 2). To visualize whether most of the variation in the SRPBS multi-disorder dataset
799 was still associated with imaging site after harmonization, we performed a PCA of functional connectivity values in the
800 harmonized SRPBS multi-disorder dataset (Fig. 7). We used the traveling-subject method for harmonization, as described in
801 the following section.

802

803 **Estimation of biases and factors**

804 The participant factor (\mathbf{p}), measurement bias (\mathbf{m}), sampling biases (\mathbf{s}_{hc} , \mathbf{s}_{mdd} , \mathbf{s}_{scz}), and psychiatric disorder factor (\mathbf{d}) were
805 estimated by fitting the regression model to the functional connectivity values of all participants from the SRPBS multi-
806 disorder dataset and the traveling-subject dataset. In this instance, vectors are denoted by lowercase bold letters (e.g., \mathbf{m}) and
807 all vectors are assumed to be column vectors. Components of vectors are denoted by subscripts such as m_k . To represent
808 participant characteristics, we used a 1-of-K binary coding scheme in which the target vector (e.g., \mathbf{x}_m) for a measurement
809 bias \mathbf{m} belonging to site k is a binary vector with all elements equal to zero—except for element k , which equals 1. If a
810 participant does not belong to any class, the target vector is a vector with all elements equal to zero. A superscript T denotes
811 the transposition of a matrix or vector, such that \mathbf{x}^T represents a row vector. For each connectivity, the regression model can
812 be written as follows:

813

$$814 \text{Connectivity} = \mathbf{x}_m^T \mathbf{m} + \mathbf{x}_{s_{hc}}^T \mathbf{s}_{hc} + \mathbf{x}_{s_{mdd}}^T \mathbf{s}_{mdd} + \mathbf{x}_{s_{scz}}^T \mathbf{s}_{scz} + \mathbf{x}_d^T \mathbf{d} + \mathbf{x}_p^T \mathbf{p} + \text{const} + e,$$

815 such that $\sum_j^9 p_j = 0, \sum_k^{12} m_k = 0, \sum_k^6 s_{hc_k} = 0, \sum_k^3 s_{mdd_k} = 0, \sum_k^3 s_{scz_k} = 0, d_1(\text{HC}) = 0,$

816 in which \mathbf{m} represents the measurement bias (12 sites \times 1), \mathbf{s}_{hc} represents the sampling bias of HCs (six sites \times 1),
 817 \mathbf{s}_{mdd} represents the sampling bias of patients with MDD (three sites \times 1), \mathbf{s}_{scz} represents the sampling bias of patients
 818 with SCZ (three sites \times 1), \mathbf{d} represents the disorder factor (3 \times 1), \mathbf{p} represents the participant factor
 819 (nine traveling subjects \times 1), $const$ represents the average functional connectivity value across all participants from all
 820 sites, and $e \sim \mathcal{N}(0, \gamma^{-1})$ represents noise. For each functional connectivity value, we estimated the respective parameters
 821 using regular ordinary least squares regression with L2 regularization, as the design matrix of the regression model is rank-
 822 deficient. When regularization was not applied, we observed spurious anticorrelation between the measurement bias and the
 823 sampling bias for HCs, and spurious correlation between the sampling bias for HCs and the sampling bias for patients with
 824 psychiatric disorders (Supplementary Figure 3a, left). These spurious correlations were also observed in the permutation data
 825 in which there were no associations between the site label and data (Supplementary Figure 3a, right). This finding suggests
 826 that the spurious correlations were caused by the rank-deficient property of the design matrix. We tuned the hyper-parameter
 827 lambda to minimize the absolute mean of these spurious correlations (Supplementary Figure 3c, left).

828

829 Analysis of contribution size

830 To quantitatively verify the magnitude relationship among factors, we calculated and compared the contribution size to
 831 determine the extent to which each bias type and factor explain the variance of the data in our linear mixed-effects model (Fig.
 832 3d). After fitting the model, the b -th connectivity from subject a can be written, as follows:

833

$$834 \text{Connectivity}_{a,b} = \mathbf{x}_m^a \mathbf{T} \mathbf{m}^b + \mathbf{x}_{s_{hc}}^a \mathbf{T} \mathbf{s}_{hc}^b + \mathbf{x}_{s_{mdd}}^a \mathbf{T} \mathbf{s}_{mdd}^b + \mathbf{x}_{s_{scz}}^a \mathbf{T} \mathbf{s}_{scz}^b + \mathbf{x}_d^a \mathbf{T} \mathbf{d}^b + \mathbf{x}_p^a \mathbf{T} \mathbf{p}^b + const + e,$$

835

836 For example, the contribution size of measurement bias (i.e., the first term) in this model was calculated as

837

838 *Contribution size_m*

$$839 = \frac{1}{N_m} \frac{1}{N_s * N} \sum_{a=1}^{N_s} \sum_{b=1}^N \frac{(\mathbf{x}_m^a \mathbf{T} \mathbf{m}^b)^2}{(\mathbf{x}_m^a \mathbf{T} \mathbf{m}^b)^2 + (\mathbf{x}_{s_{hc}}^a \mathbf{T} \mathbf{s}_{hc}^b)^2 + (\mathbf{x}_{s_{mdd}}^a \mathbf{T} \mathbf{s}_{mdd}^b)^2 + (\mathbf{x}_{s_{scz}}^a \mathbf{T} \mathbf{s}_{scz}^b)^2 + (\mathbf{x}_d^a \mathbf{T} \mathbf{d}^b)^2 + (\mathbf{x}_p^a \mathbf{T} \mathbf{p}^b)^2 + e^2},$$

840

841 in which N_m represents the number of components for each factor, N represents the number of connectivities, N_s
 842 represents the number of subjects, and *Contribution size_m* represents the magnitude of the contribution size of
 843 measurement bias. These formulas were used to assess the contribution sizes of individual factors related to measurement bias
 844 (e.g., phase-encoding direction, scanner, coil, and fMRI manufacturer: Fig. 5b). We decomposed the measurement bias into
 845 these factors, after which the relevant parameters were estimated. Other parameters were fixed at the same values as previously
 846 estimated.

847

848 Spatial characteristics of measurement bias, sampling bias, and each factor in the brain

849 To evaluate the spatial characteristics of each type of bias and each factor in the brain, we calculated the magnitude of the
 850 effect on each ROI. First, we calculated the median absolute value of the effect on each functional connection among sites or
 851 participants for each bias and participant factor. We then calculated the absolute value of each connection for each disorder

852 factor. The uppercase bold letters (e.g., \mathbf{M}) and subscript vectors (e.g., \mathbf{m}_k) represent the vectors for the number of functional
853 connections:

854

$$855 \quad \mathbf{M} = \text{median}(|\mathbf{m}_k|), \mathbf{S}_{hc} = \text{median}(|s_{hc_k}|), \mathbf{S}_{mdd} = \text{median}(|s_{mdd_k}|), \mathbf{S}_{scz} = \text{median}(|s_{scz_k}|), \mathbf{D}_2 = |\mathbf{d}_2|, \mathbf{D}_3 = |\mathbf{d}_3|, \mathbf{P} = \text{median}(|\mathbf{p}_j|)$$

856

857 We next calculated the magnitude of the effect on ROIs as the average connectivity value between all ROIs, except for
858 themselves.

859

$$860 \quad Effect_on_ROI_n = \frac{1}{N_{ROI} - 1} \sum_{v \neq n}^{N_{ROI}} Effect_on_connectivity_{n,v},$$

861

862 in which N_{ROI} represents the number of ROIs, $Effect_on_ROI_n$ represents the magnitude of the effect on the n -th ROI, and
863 $Effect_on_connectivity_{n,v}$ represents the magnitude of the effect on connectivity between the n -th ROI and v -th ROI.

864

865 **Hierarchical clustering analysis for measurement bias**

866 We calculated the Pearson's correlation coefficients among measurement biases \mathbf{m}_k ($N \times$
867 1, where N is the number of functional connections) for each site k , and performed a hierarchical clustering analysis
868 based on the correlation coefficients across measurement biases. To visualize the dendrogram (Fig. 5), we used the
869 “*dendrogram*”, “*linkage*”, and “*optimalleaforder*” functions in MATLAB (R2015a, Mathworks, USA).

870

871

872 **Comparison of models for sampling bias**

873 We investigated whether sampling bias is caused by the differences in the number of participants among imaging sites, or by
874 sampling from different populations among imaging sites. We constructed two models and investigated which model provides
875 the best explanation of sampling bias. In the single-population model, we assumed that participants were sampled from a single
876 population across imaging sites. In the different-population model, we assumed that participants were sampled from different
877 populations among imaging sites. We first theorized how the number of participants at each site affects the variance of
878 sampling biases across connectivity values, as follows:

879 In the *single-population model*, we assumed that the functional connectivity values of each participant were
880 generated from an independent Gaussian distribution, with a mean of 0 and a variance of ξ^2 for each connectivity value.
881 Then, the functional connectivity vector for participant j at site k can be described as

882

$$883 \quad \mathbf{c}_j^k \sim \mathcal{N}(\mathbf{0}, \xi^2 \mathbf{I}).$$

884

885 Let \mathbf{c}_k be the vector of functional connectivity at site k averaged across participants. In this model, \mathbf{c}_k represents the
886 sampling bias and can be described as

887

$$887 \quad \mathbf{c}_k = \frac{1}{N_k} \sum_{j=1}^{N_k} \mathbf{c}_j^k \sim \mathcal{N}\left(\mathbf{0}, \frac{\xi^2}{N_k} \mathbf{I}\right),$$

888 in which N_k represents the number of participants at site k . The variance across functional connectivity values for \mathbf{c}_k is

889 described as

$$890 \quad V_k = \frac{1}{N} \sum_{i=1}^N (c_{ki} - \bar{c}_k)^2 = \frac{1}{N} \mathbf{c}_k^T \left(\mathbf{I} - \frac{1}{N} \mathbf{1}\mathbf{1}' \right)^T \left(\mathbf{I} - \frac{1}{N} \mathbf{1}\mathbf{1}' \right) \mathbf{c}_k \approx \frac{1}{N} \mathbf{c}_k^T \mathbf{c}_k,$$

891 in which $\mathbf{1}$ represents the $N \times 1$ vector of ones and \mathbf{I} represents the $N \times N$ identity matrix. Since N equals 35,778 and
892 $\frac{1}{35778}$ is sufficiently smaller than 1, we can approximate

$$893 \quad \mathbf{I} - \frac{1}{N} \mathbf{1}\mathbf{1}' \approx \mathbf{I}.$$

894 Then, the expected value of variance across functional connectivity values for sampling-bias can be described as

$$895 \quad \mathbb{E}[V_k] \approx \frac{1}{N} \mathbb{E}[\mathbf{c}_k^T \mathbf{c}_k] = \frac{1}{N} \text{Tr} \left(\frac{\xi^2}{N_k} \mathbf{I} \right) = \frac{\xi^2}{N_k}.$$

896

897 In the different-population model, we assumed that the functional connectivity values of each participant were
898 generated from a different independent Gaussian distribution, with an average of β_k and a variance of ξ^2 depending on the
899 population of each site. In this situation, the functional connectivity vector for participant j at site k can be described as

$$900 \quad \mathbf{c}_j^k \sim \mathcal{N}(\beta_k, \xi^2 \mathbf{I}).$$

901 Here, we assume that the average of the population β_k is sampled from an independent Gaussian distribution with an average
902 of 0 and a variance of σ^2 . That is, β_k is expressed as

903

$$904 \quad \beta_k \sim \mathcal{N}(\mathbf{0}, \sigma^2 \mathbf{I}).$$

905

906 The vector of functional connectivity for site k averaged across participants can then be described as

$$907 \quad \mathbf{c}_k \sim \mathcal{N} \left(\mathbf{0}, \left(\frac{\xi^2}{N_k} + \sigma^2 \right) \mathbf{I} \right).$$

908 The variance across functional connectivity values for \mathbf{c}_k can be described as

$$909 \quad \mathbb{E}[V_k] \approx \frac{\xi^2}{N_k} + \sigma^2.$$

910

911 In summary, the variance of sampling bias across functional connectivity values in each model is expressed by the
912 number of participants at a given site, as follows:

913

$$914 \quad \text{single-population model: } y_k = -x_k + 2 \log_{10} \xi$$

915

$$916 \quad \text{different-population model: } y_k = -\log_{10}(\xi^2 10^{-x_k} + \sigma^2),$$

917

918 in which $y_k = \log_{10}(v_k)$, v_k represents the variance across functional connectivity values for \mathbf{s}_{hc_k} , \mathbf{s}_{hc_k} represents the
919 sampling bias of HCs at site k ($N \times 1$: N is the number of functional connectivity), $x_k = \log_{10}(N_k)$, and N_k
920 represents the number of participants at site k . We estimated the parameters ξ and σ using the MATLAB (R2015a,
921 Mathworks, USA) optimization function “*fminunc*”. To simplify statistical analyses, sampling bias was estimated based on
922 functional connectivity in which the average across all participants was set to zero.

923 We aimed to determine which model provided the best explanation of sampling bias in our data by calculating the
924 corrected Akaike information criterion (AICc; under the assumption of a Gaussian distribution) for small-sample data [36, 37],
925 as well as BIC:
926

$$927 \quad \text{AICc} = \sum_{k=1}^6 \ln \varphi_k^2 + 2q + \frac{2q(q+1)}{(6-q-1)},$$

$$928 \quad \text{BIC} = \sum_{k=1}^6 \ln \varphi_k^2 + q * \log(6),$$

929
930 in which $\varphi_k = v_k - \widehat{v}_k$, \widehat{v}_k represents the estimated variance, and q represents the number of parameters in each model (1
931 or 2).

932 To investigate prediction performance, we used leave-one-site-out-cross-validation in which we estimated the
933 parameters ξ and σ using data from five sites. The variance of sampling bias was predicted based on the number of
934 participants at the remaining site. This procedure was repeated to predict variance values for sampling bias at all six sites. We
935 then calculated the absolute errors between predicted and actual variances for all sites.

936 937 **Harmonization procedures**

938 We compared four different harmonization methods for the removal of site differences, as described in the main text.

939 940 *Traveling-subject harmonization*

941 Measurement biases were estimated by fitting the regression model to the combined SRPBS multi-disorder and traveling-
942 subject datasets in the same way in “Estimation of biases and factors” section. For each connectivity, the regression model can
943 be written as follows:

$$944 \quad \text{Connectivity} = \mathbf{x}_m^T \mathbf{m} + \mathbf{x}_{shc}^T \mathbf{s}_{shc} + \mathbf{x}_{smd}^T \mathbf{s}_{smd} + \mathbf{x}_{scz}^T \mathbf{s}_{scz} + \mathbf{x}_d^T \mathbf{d} + \mathbf{x}_p^T \mathbf{p} + \text{const} + e. \quad (1)$$

945
946
947 Measurement bias were removed by subtracting the estimated measurement biases. Thus, the harmonized functional
948 connectivity values were set, as follows:

$$949 \quad \text{Connectivity}^{\text{Traveling-subje}} = \text{Connectivity} - \mathbf{x}_m^T \widehat{\mathbf{m}},$$

950
951
952 in which $\widehat{\mathbf{m}}$ represents the estimated measurement bias.

953 954 *GLM harmonization*

955 The GLM harmonization method adjusts the functional connectivity value for site difference using GLM. Site differences were
956 estimated by fitting the regression model, which included site label only, to the SRPBS multi-disorder dataset only. The
957 regression model can be written as

$$958 \quad \text{Connectivity} = \text{const} + \mathbf{x}_s^T \mathbf{s}^{\text{GLM}} + e, \quad (2)$$

960

961 in which \mathbf{s}^{GLM} represents the site difference (nine sites \times 1). For each functional connectivity value, we estimated the
 962 parameters using regular ordinary least squares regression. Site differences were removed by subtracting the estimated site
 963 differences. Thus, the harmonized functional connectivity values were set, as follows:

964

$$965 \quad \text{Connectivity}^{GLM} = \text{Connectivity} - \mathbf{x}_s^T \widehat{\mathbf{s}}^{GLM},$$

966

967 in which $\widehat{\mathbf{s}}^{GLM}$ represents the estimated site difference.

968

969 *Adjusted GLM harmonization*

970 Site differences were estimated by fitting the regression model, which included site label and diagnosis label, to the SRPBS
 971 multi-disorder dataset. The regression model can be written as

972

$$973 \quad \text{Connectivity} = \text{const} + \mathbf{x}_s^T \mathbf{s}^{Adj} + \mathbf{x}_d^T \mathbf{d}^{Adj} + \mathbf{e}, \quad (3)$$

974

975 In which \mathbf{s}^{Adj} represents the site difference (nine sites \times 1). For each functional connectivity value, we estimated the
 976 parameters via regular ordinary least squares regression. Site differences were removed by subtracting the estimated site
 977 difference only. Thus, the harmonized functional connectivity values were set, as follows:

978

$$979 \quad \text{Connectivity}^{Adj} = \text{Connectivity} - \mathbf{x}_s^T \widehat{\mathbf{s}}^{Adj},$$

980

981 in which $\widehat{\mathbf{s}}^{Adj}$ represents the estimated site difference.

982

983 *ComBat harmonization*

984 The ComBat harmonization model [16, 17, 19, 38] extends the adjusted GLM harmonization method in two ways: (1) it models
 985 site-specific scaling factors and (2) it uses empirical Bayesian criteria to improve the estimation of site parameters for small
 986 sample sizes. The model assumes that the expected connectivity value can be modeled as a linear combination of the biological
 987 variables and the site differences in which the error term is modulated by additional site-specific scaling factors.

988

$$989 \quad \text{Connectivity} = \text{const} + \mathbf{x}_s^T \mathbf{s}^{ComBat} + \mathbf{x}_d^T \mathbf{d}^{ComBat} + \delta_k \mathbf{e}, \quad (4)$$

990

991 in which \mathbf{s}^{ComBat} represents the site difference (nine sites \times 1), and δ_k represents the scale parameter for site differences at
 992 site k for the respective connectivity value. The harmonized functional connectivity values were set, as follows:

993

$$995 \quad \text{Connectivity}^{ComBat} = \frac{\text{Connectivity} - \text{const} - \mathbf{x}_s^T \widehat{\mathbf{s}}^{ComBat} - \mathbf{x}_d^T \widehat{\mathbf{d}}^{ComBat}}{\widehat{\delta}_k} + \text{const} + \mathbf{x}_d^T \widehat{\mathbf{d}}^{ComBat},$$

994

996 in which $\widehat{\delta}_k$, $\widehat{\mathbf{d}}^{ComBat}$, and $\widehat{\mathbf{s}}^{ComBat}$ are the empirical Bayes estimates of δ_k , \mathbf{d}^{ComBat} , and \mathbf{s}^{ComBat} , respectively using
 997 “combat” function in <https://github.com/Jfortin1/ComBatHarmonization>. Thus, ComBat simultaneously models and estimates

998 biological and nonbiological terms and algebraically removes the estimated additive and multiplicative site differences. Of
999 note, in the ComBat model, we included diagnosis as covariates to preserve important biological trends in the data and avoid
1000 overcorrection.

1001

1002 **2-fold cross-validation evaluation procedure**

1003 We compared four different harmonization methods for the removal of site difference or measurement bias by 2-fold cross-
1004 validation, as described in the main text. In the traveling-subject harmonization method, we estimated the measurement bias
1005 by applying the regression model written in equation (1) in “Harmonization procedures” section to the estimating dataset. Thus,
1006 the harmonized functional connectivity values in testing dataset were set, as follows:

$$1007 \text{connectivity}_{\text{testing dataset}}^{\text{Traveling-subje}} = \text{Connectivity}_{\text{testing dataset}} - \mathbf{x}_m^T \hat{\mathbf{m}}_{\text{estimating dataset}},$$

1008 in which $\hat{\mathbf{m}}_{\text{estimating dataset}}$ represents the estimated measurement bias using the estimating dataset.

1009 By contrast, in the other harmonization methods, we estimated the site differences by applying the regression models written
1010 in equations (2)–(4) in “Harmonization procedures” section to the estimating dataset (fold1 data). Thus, the harmonized
1011 functional connectivity values in testing dataset were set, as follows:

$$1012 \text{connectivity}_{\text{testing dataset}}^{\text{GLM}} = \text{Connectivity}_{\text{testing dataset}} - \mathbf{x}_s^T \widehat{\mathbf{s}}_{\text{fold1}}^{\text{GLM}},$$

$$1013 \text{connectivity}_{\text{testing dataset}}^{\text{Adj}} = \text{Connectivity}_{\text{testing dataset}} - \mathbf{x}_s^T \widehat{\mathbf{s}}_{\text{fold1}}^{\text{Adj}},$$

$$1014 \text{connectivity}_{\text{testing dataset}}^{\text{ComBat}} = \text{Connectivity}_{\text{testing dataset}} - \mathbf{x}_s^T \widehat{\mathbf{s}}_{\text{fold1}}^{\text{ComBat}},$$

1015 in which $\widehat{\mathbf{s}}_{\text{fold1}}^{\text{GLM}}, \widehat{\mathbf{s}}_{\text{fold1}}^{\text{Adj}}, \widehat{\mathbf{s}}_{\text{fold1}}^{\text{ComBat}}$ represents the estimated site differences using fold1 data.

1016 We then estimated the measurement bias, participant factor, and disorder factors by applying the regression model written in
1017 equation (1) to the harmonized functional connectivity values in the testing dataset. Finally, we evaluated the standard
1018 deviation of the magnitude distribution of measurement bias calculated in the same way as described in “Quantification of site
1019 differences” section among the harmonization methods. This procedure was done again by exchanging the estimating dataset
1020 and the testing dataset.

1021

1022 **Code availability:** All codes used for the analyses are available from the authors on request.

1023 **Data availability:** All relevant data are available from the authors on request. All data can be downloaded publicly from the
1024 following site: <https://bicr-resource.atr.jp/decnefpro/>.

1025 **Acknowledgements:** This study was conducted under the “Development of BMI Technologies for Clinical Application” of
1026 the Strategic Research Program for Brain Sciences, and the contract research Grant Number JP18dm0307008 supported by
1027 the Japan Agency for Medical Research and Development (AMED). This study was also partially supported by the ImPACT
1028 Program of the Council for Science, Technology and Innovation (Cabinet Office, Government of Japan). H.I. was partially
1029 supported by JSPS KAKENHI 26120002.

1030 **Author contributions:** A.Y., N.Y., and H.I. designed the study. N.Y., T.I., T.Y., N.I., M.T., Y.Y., A.K., N.O., T.Y., K.M.,
1031 R.H., G.O., Y.S., J.N., Y.S., K.K., N.K., H.T., Y.O. and S.T. recruited participants of the study, collected their clinical and
1032 imaging data and constructed the database. A.Y. performed data preprocessing and data analysis under the super vision of
1033 G.L., J.M., O.Y., M.K., and H.I., and A.Y., O.Y., M.K. and H.I. primarily wrote the manuscript.

1034 **Competing financial interests:** The authors declare no competing financial interests.

1035

1036

1037 **Reference**

- 1038 1. Glasser MF, Smith SM, Marcus DS, Andersson JL, Auerbach EJ, Behrens TE, et al. The Human Connectome
1039 Project's neuroimaging approach. *Nat Neurosci.* 2016;19(9):1175-87. doi: 10.1038/nn.4361. PubMed PMID:
1040 27571196.
- 1041 2. Yamada T, Hashimoto RI, Yahata N, Ichikawa N, Yoshihara Y, Okamoto Y, et al. Resting-State Functional
1042 Connectivity-Based Biomarkers and Functional MRI-Based Neurofeedback for Psychiatric Disorders: A
1043 Challenge for Developing Theranostic Biomarkers. *Int J Neuropsychopharmacol.* 2017;20(10):769-81. doi:
1044 10.1093/ijnp/pyx059. PubMed PMID: 28977523; PubMed Central PMCID: PMC5632305.
- 1045 3. Biswal BB, Mennes M, Zuo XN, Gohel S, Kelly C, Smith SM, et al. Toward discovery science of human brain
1046 function. *Proc Natl Acad Sci U S A.* 2010;107(10):4734-9. doi: 10.1073/pnas.0911855107. PubMed PMID:
1047 20176931; PubMed Central PMCID: PMC2842060.
- 1048 4. Woo CW, Chang LJ, Lindquist MA, Wager TD. Building better biomarkers: brain models in translational
1049 neuroimaging. *Nat Neurosci.* 2017;20(3):365-77. doi: 10.1038/nn.4478. PubMed PMID: 28230847.
- 1050 5. Xia M, He Y. Functional connectomics from a "big data" perspective. *NeuroImage.* 2017;160:152-67. doi:
1051 10.1016/j.neuroimage.2017.02.031. PubMed PMID: 28232122.
- 1052 6. Di Martino A, Yan CG, Li Q, Denio E, Castellanos FX, Alaerts K, et al. The autism brain imaging data
1053 exchange: towards a large-scale evaluation of the intrinsic brain architecture in autism. *Mol Psychiatry.*
1054 2014;19(6):659-67. doi: 10.1038/mp.2013.78. PubMed PMID: 23774715; PubMed Central PMCID:
1055 PMC4162310.
- 1056 7. Pearson G. Multisite collaborations and large databases in psychiatric neuroimaging: advantages, problems,
1057 and challenges. *Schizophr Bull.* 2009;35(1):1-2. doi: 10.1093/schbul/sbn166. PubMed PMID: 19023121;
1058 PubMed Central PMCID: PMC2643967.
- 1059 8. Yahata N, Kasai K, Kawato M. Computational neuroscience approach to biomarkers and treatments for mental
1060 disorders. *Psychiatry Clin Neurosci.* 2017;71(4):215-37. doi: 10.1111/pcn.12502. PubMed PMID: 28032396.
- 1061 9. Takagi Y, Sakai Y, Lisi G, Yahata N, Abe Y, Nishida S, et al. A Neural Marker of Obsessive-Compulsive
1062 Disorder from Whole-Brain Functional Connectivity. *Sci Rep.* 2017;7(1):7538. Epub 2017/08/10. doi:
1063 10.1038/s41598-017-07792-7. PubMed PMID: 28790433; PubMed Central PMCID: PMC5548868.
- 1064 10. Yahata N, Morimoto J, Hashimoto R, Lisi G, Shibata K, Kawakubo Y, et al. A small number of abnormal
1065 brain connections predicts adult autism spectrum disorder. *Nat Commun.* 2016;7:11254. Epub 2016/04/15. doi:
1066 10.1038/ncomms11254. PubMed PMID: 27075704; PubMed Central PMCID: PMC4834637.
- 1067 11. Abraham A, Milham MP, Di Martino A, Craddock RC, Samaras D, Thirion B, et al. Deriving reproducible
1068 biomarkers from multi-site resting-state data: An Autism-based example. *NeuroImage.* 2017;147:736-45. doi:
1069 10.1016/j.neuroimage.2016.10.045. PubMed PMID: 27865923.
- 1070 12. Nieuwenhuis M, Schnack HG, van Haren NE, Lappin J, Morgan C, Reinders AA, et al. Multi-center MRI
1071 prediction models: Predicting sex and illness course in first episode psychosis patients. *NeuroImage.*
1072 2017;145(Pt B):246-53. doi: 10.1016/j.neuroimage.2016.07.027. PubMed PMID: 27421184; PubMed Central
1073 PMCID: PMC5193177.
- 1074 13. Orban P, Dansereau C, Desbois L, Mongeau-Perusse V, Giguere CE, Nguyen H, et al. Multisite

- 1075 generalizability of schizophrenia diagnosis classification based on functional brain connectivity. *Schizophrenia*
1076 *research*. 2018;192:167-71. Epub 2017/06/12. doi: 10.1016/j.schres.2017.05.027. PubMed PMID: 28601499.
- 1077 14. Dansereau C, Benhajali Y, Risterucci C, Pich EM, Orban P, Arnold D, et al. Statistical power and prediction
1078 accuracy in multisite resting-state fMRI connectivity. *NeuroImage*. 2017;149:220-32. doi:
1079 10.1016/j.neuroimage.2017.01.072. PubMed PMID: 28161310.
- 1080 15. Watanabe T, Sasaki Y, Shibata K, Kawato M. Advances in fMRI Real-Time Neurofeedback. *Trends Cogn*
1081 *Sci*. 2017;21(12):997-1010. doi: 10.1016/j.tics.2017.09.010. PubMed PMID: 29031663; PubMed Central
1082 PMCID: PMC5694350.
- 1083 16. Fortin JP, Cullen N, Sheline YI, Taylor WD, Aselcioglu I, Cook PA, et al. Harmonization of cortical thickness
1084 measurements across scanners and sites. *NeuroImage*. 2017;167:104-20. doi:
1085 10.1016/j.neuroimage.2017.11.024. PubMed PMID: 29155184.
- 1086 17. Fortin JP, Parker D, Tunc B, Watanabe T, Elliott MA, Ruparel K, et al. Harmonization of multi-site diffusion
1087 tensor imaging data. *NeuroImage*. 2017;161:149-70. doi: 10.1016/j.neuroimage.2017.08.047. PubMed PMID:
1088 28826946; PubMed Central PMCID: PMC5736019.
- 1089 18. Rao A, Monteiro JM, Mourao-Miranda J, Alzheimer's Disease I. Predictive modelling using neuroimaging
1090 data in the presence of confounds. *NeuroImage*. 2017;150:23-49. doi: 10.1016/j.neuroimage.2017.01.066.
1091 PubMed PMID: 28143776; PubMed Central PMCID: PMC5391990.
- 1092 19. Yu M, Linn KA, Cook PA, Phillips ML, McInnis M, Fava M, et al. Statistical harmonization corrects site
1093 effects in functional connectivity measurements from multi-site fMRI data. *Hum Brain Mapp*. 2018. doi:
1094 10.1002/hbm.24241. PubMed PMID: 29962049.
- 1095 20. Noble S, Scheinost D, Finn ES, Shen X, Papademetris X, McEwen SC, et al. Multisite reliability of MR-based
1096 functional connectivity. *NeuroImage*. 2017;146:959-70. doi: 10.1016/j.neuroimage.2016.10.020. PubMed
1097 PMID: 27746386; PubMed Central PMCID: PMC5322153.
- 1098 21. Benazzi F. Various forms of depression. *Dialogues in Clinical Neuroscience*. 2006;8(2):151-61. PubMed
1099 PMID: PMC3181770.
- 1100 22. Drysdale AT, Grosenick L, Downar J, Dunlop K, Mansouri F, Meng Y, et al. Resting-state connectivity
1101 biomarkers define neurophysiological subtypes of depression. *Nat Med*. 2017;23(1):28-38. doi:
1102 10.1038/nm.4246. PubMed PMID: 27918562; PubMed Central PMCID: PMC5624035.
- 1103 23. Ng B, Dressler M, Varoquaux G, Poline JB, Greicius M, Thirion B. Transport on Riemannian manifold for
1104 functional connectivity-based classification. *Medical image computing and computer-assisted intervention :
1105 MICCAI International Conference on Medical Image Computing and Computer-Assisted Intervention*.
1106 2014;17(Pt 2):405-12. Epub 2014/12/09. PubMed PMID: 25485405.
- 1107 24. Finn ES, Shen X, Scheinost D, Rosenberg MD, Huang J, Chun MM, et al. Functional connectome
1108 fingerprinting: identifying individuals using patterns of brain connectivity. *Nat Neurosci*. 2015;18(11):1664-
1109 71. doi: 10.1038/nn.4135. PubMed PMID: 26457551; PubMed Central PMCID: PMC5008686.
- 1110 25. Rosenberg MD, Finn ES, Scheinost D, Papademetris X, Shen X, Constable RT, et al. A neuromarker of
1111 sustained attention from whole-brain functional connectivity. *Nat Neurosci*. 2016;19(1):165-71. doi:
1112 10.1038/nn.4179. PubMed PMID: 26595653; PubMed Central PMCID: PMC54696892.
- 1113 26. Shen X, Tokoglu F, Papademetris X, Constable RT. Groupwise whole-brain parcellation from resting-state

- 1114 fMRI data for network node identification. *NeuroImage*. 2013;82:403-15. doi:
1115 10.1016/j.neuroimage.2013.05.081. PubMed PMID: 23747961; PubMed Central PMCID: PMC3759540.
- 1116 27. Noble S, Spann MN, Tokoglu F, Shen X, Constable RT, Scheinost D. Influences on the Test-Retest Reliability
1117 of Functional Connectivity MRI and its Relationship with Behavioral Utility. *Cereb Cortex*. 2017;27(11):5415-
1118 29. doi: 10.1093/cercor/bhx230. PubMed PMID: 28968754.
- 1119 28. Jezzard P, Clare S. Sources of distortion in functional MRI data. *Hum Brain Mapp*. 1999;8(2-3):80-5. Epub
1120 1999/10/19. PubMed PMID: 10524596.
- 1121 29. Weiskopf N, Hutton C, Josephs O, Deichmann R. Optimal EPI parameters for reduction of susceptibility-
1122 induced BOLD sensitivity losses: a whole-brain analysis at 3 T and 1.5 T. *NeuroImage*. 2006;33(2):493-504.
1123 doi: 10.1016/j.neuroimage.2006.07.029. PubMed PMID: 16959495.
- 1124 30. Kaiser RH, Andrews-Hanna JR, Wager TD, Pizzagalli DA. Large-Scale Network Dysfunction in Major
1125 Depressive Disorder: A Meta-analysis of Resting-State Functional Connectivity. *JAMA Psychiatry*.
1126 2015;72(6):603-11. doi: 10.1001/jamapsychiatry.2015.0071. PubMed PMID: 25785575; PubMed Central
1127 PMCID: PMC4456260.
- 1128 31. Mulders PC, van Eijndhoven PF, Schene AH, Beckmann CF, Tendolkar I. Resting-state functional
1129 connectivity in major depressive disorder: A review. *Neurosci Biobehav Rev*. 2015;56:330-44. doi:
1130 10.1016/j.neubiorev.2015.07.014. PubMed PMID: 26234819.
- 1131 32. Kuhn S, Gallinat J. Resting-state brain activity in schizophrenia and major depression: a quantitative meta-
1132 analysis. *Schizophr Bull*. 2013;39(2):358-65. doi: 10.1093/schbul/sbr151. PubMed PMID: 22080493; PubMed
1133 Central PMCID: PMC3576173.
- 1134 33. Li T, Wang Q, Zhang J, Rolls ET, Yang W, Palaniyappan L, et al. Brain-Wide Analysis of Functional
1135 Connectivity in First-Episode and Chronic Stages of Schizophrenia. *Schizophr Bull*. 2017;43(2):436-48. doi:
1136 10.1093/schbul/sbw099. PubMed PMID: 27445261; PubMed Central PMCID: PMC45605268.
- 1137 34. Minzenberg MJ, Laird AR, Thelen S, Carter CS, Glahn DC. Meta-analysis of 41 functional neuroimaging
1138 studies of executive function in schizophrenia. *Archives of general psychiatry*. 2009;66(8):811-22. Epub
1139 2009/08/05. doi: 10.1001/archgenpsychiatry.2009.91. PubMed PMID: 19652121; PubMed Central PMCID:
1140 PMC2888482.
- 1141 35. Anderson JS, Nielsen JA, Froehlich AL, DuBray MB, Druzgal TJ, Cariello AN, et al. Functional connectivity
1142 magnetic resonance imaging classification of autism. *Brain*. 2011;134(Pt 12):3742-54. doi:
1143 10.1093/brain/awr263. PubMed PMID: 22006979; PubMed Central PMCID: PMC3235557.
- 1144 36. Burnham KP, Anderson DR. Model selection and multimodel inference: a practical information-theoretic
1145 approach: Springer Science & Business Media; 2003.
- 1146 37. Cortese A, Amano K, Koizumi A, Kawato M, Lau H. Multivoxel neurofeedback selectively modulates
1147 confidence without changing perceptual performance. *Nat Commun*. 2016;7:13669. doi:
1148 10.1038/ncomms13669. PubMed PMID: 27976739; PubMed Central PMCID: PMC45171844 inventor of
1149 patents related to the neurofeedback method used in this study, and the original assignee of the patents is ATR,
1150 with which M.K. is affiliated. The remaining authors declare no competing financial interests.
- 1151 38. Johnson WE, Li C, Rabinovic A. Adjusting batch effects in microarray expression data using empirical Bayes
1152 methods. *Biostatistics*. 2007;8(1):118-27. doi: 10.1093/biostatistics/kxj037. PubMed PMID: 16632515.

- 1153 39. Hutton C, Bork A, Josephs O, Deichmann R, Ashburner J, Turner R. Image distortion correction in fMRI: A
1154 quantitative evaluation. *NeuroImage*. 2002;16(1):217-40. doi: 10.1006/nimg.2001.1054. PubMed PMID:
1155 11969330.
- 1156 40. Jenkinson M. Fast, automated, N-dimensional phase-unwrapping algorithm. *Magn Reson Med*.
1157 2003;49(1):193-7. doi: 10.1002/mrm.10354. PubMed PMID: 12509838.
- 1158 41. Jezzard P, Balaban RS. Correction for geometric distortion in echo planar images from B0 field variations.
1159 *Magn Reson Med*. 1995;34(1):65-73. Epub 1995/07/01. PubMed PMID: 7674900.
- 1160 42. Andersson JLR, Skare S, Ashburner J. How to correct susceptibility distortions in spin-echo echo-planar
1161 images: application to diffusion tensor imaging. *NeuroImage*. 2003;20(2):870-88. doi: 10.1016/s1053-
1162 8119(03)00336-7.
- 1163 43. Wang S, Peterson DJ, Gatenby JC, Li W, Grabowski TJ, Madhyastha TM. Evaluation of Field Map and
1164 Nonlinear Registration Methods for Correction of Susceptibility Artifacts in Diffusion MRI. *Front Neuroinform*.
1165 2017;11:17. doi: 10.3389/fninf.2017.00017. PubMed PMID: 28270762; PubMed Central PMCID:
1166 PMC5318394.
- 1167 44. Ciric R, Wolf DH, Power JD, Roalf DR, Baum GL, Ruparel K, et al. Benchmarking of participant-level
1168 confound regression strategies for the control of motion artifact in studies of functional connectivity.
1169 *NeuroImage*. 2017;154:174-87. doi: 10.1016/j.neuroimage.2017.03.020. PubMed PMID: 28302591; PubMed
1170 Central PMCID: PMC5483393.
- 1171 45. Power JD, Barnes KA, Snyder AZ, Schlaggar BL, Petersen SE. Spurious but systematic correlations in
1172 functional connectivity MRI networks arise from subject motion. *NeuroImage*. 2012;59(3):2142-54. doi:
1173 10.1016/j.neuroimage.2011.10.018. PubMed PMID: 22019881; PubMed Central PMCID: PMC3254728.
1174